Fundamental Studies on the Structures and Spectroscopic Properties of Imidazo[1,2-*a*]pyrazin-3(7*H*)-one Derivatives

Shunichiro Nakai, Masanori Yasui, Masaki Nakazato,[†] **Fujiko Iwasaki, Shojiro Maki,**
Haruki Niwa, Mamoru Ohashi,[††] **and Takashi Hirano**[*]

Department of Applied Physics and Chemistry, The University of Electro-Communications,
Chofu, Tokyo 182-8585

†Center for Instrumental Analysis, The University of Electro-Communications, Chofu, Tokyo 182-8585

††Department of Materials Science, Kanagawa University, Hiratsuka, Kanagawa 259-1293

Received May 21, 2003; E-mail: hirano@pc.uec.ac.jp

The fundamental physical properties of 2-methyl and 2-phenylimidazo[1,2-*a*]pyrazin-3(7*H*)-one **1** and **2**, and their *N*- and *O*-alkylated derivatives **3–6** have been investigated by X-ray crystallography, UV/vis absorption spectroscopy, NMR, and AM1-COSMO calculations. The crystal structures of **3** and **4** showed that the imidazo[1,2-*a*]pyrazin-3(7*H*)-one (imidazopyrazinone) π-system has a planar ring structure and a weakened carbonyl character of the C3–O10 bond, suggesting that the imidazopyrazinone π-system has the character of a zwitter-ionic resonance structure to increase the aromaticity. The data concerning the bond length alternations and the NMR chemical shifts of **1–4** also support that their imidazopyrazinone rings have small portions of aromatic character. In addition, imidazopyrazinone derivatives **1–4** showed solvatochromism originating by hydrogen-bonding interactions with hydrogen-bond donor solvent molecules; derivatives **1** and **2** prefer to be the NH form isomers in their tautomeric equilibriums. These observations were consistently evaluated by MO calculations. The physical properties of protonated species of **1–6** and anion species of **1** and **2** were also established. The fundamental properties of the imidazopyrazinone π-system explain the several problems of the chemi- and bioluminescence reactivities of imidazopyrazinone derivatives and of the construction of a bioluminescent supramolecule.

The imidazo[1,2-*a*]pyrazin-3(7*H*)-one (imidazopyrazinone) ring system is a core structure of the luminescent substrates isolated from marine bioluminescent organisms, such as the jellyfish *Aequorea*,[1,2] the crustacea *Vargula* (*Cypridina*),[3–5] and the luminous squid *Symplectoteuthis*.[6] During a bioluminescence reaction, an imidazopyrazinone substrate reacts with O_2 in an enzymatic process, to give an excited amidopyrazine derivative which emits light.[7–9] To establish the mechanism of *Aequorea* bioluminescence, we have systematically investigated the bio- and chemiluminescent reactivities of imidazopyrazinone derivatives. For instance, a substituent effect on the bio- and chemiluminescent properties of imidazopyrazinone derivatives has been studied to obtain information about a correlation between the reactivity and physical properties of imidazopyrazinone derivatives.[10] These studies make us seek to systematically understand the fundamental physical properties of imidazopyrazinone derivatives.[11] Furthermore, imidazopyrazinone derivatives are also interesting compounds as antioxidant reagents from the viewpoint of medicinal chemistry.[12] The antioxidative properties of imidazopyrazinone derivatives would also be related to their physical properties.

The physical properties of the imidazopyrazinone π-system were well investigated in a pioneering study by Goto et al.[13] They studied the UV/vis absorption, NMR, mass, and IR spectroscopic characteristics of imidazopyrazinone derivatives, and reported on their fundamental physical characteristics accompanied by problems of protonation, deprotonation, and tauto-

meric isomerization. After studies by the Goto group, several groups reported on the physical properties of imidazopyrazinone derivatives characterized by UV/vis absorption spectra,[14,15] NMR,[12a] and X-ray crystallographic analysis.[12a] These studies, however, showed no systematic comparison with the data of Goto's reports, and made some confusion about the fundamental physical properties of imidazopyrazinone derivatives. Furthermore, there has been no characterization of the imidazopyrazinone π-system from a molecular orbital consideration.

In the present work, we systematically reinvestigated the fundamental physical properties of the imidazopyrazinone π-system by X-ray crystallography, UV/vis absorption spectroscopy, and NMR. For this research, we adopted simple imidazopyrazinone derivatives, **1** and **2**, and their *N*- and *O*-alkyl derivatives **3–6**. Alkyl derivatives **3–6** are useful to confirm the fundamental property of the π-system, since the tautomeric isomerization of **3–6** is inhibited. The observed physical properties of imidazopyrazinone derivatives have been evaluated by comparing with the reported data of the Goto group and others. Furthermore, we tried to correlate the physical properties of the imidazopyrazinone π-system to the results of molecular-orbital calculations. Based on the fundamental properties of the imidazopyrazinone π-systems, we would like to report here about the problems of aromaticity of the imidazopyrazinone ring system, tautomeric isomerization, protonation/deprotonation, and chemi- and bioluminescence reactivities.
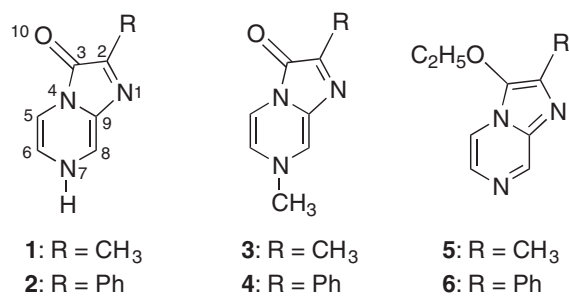
Chart 1.

tions gave O-ethylated products **5** and **6** in 52 and 46% yields, respectively, accompanied by *N*-ethyl products.

2. X-ray Crystal Structure.   X-ray crystal structures of protonated species of **1** and a neutral form of **2** with crystal waters were reported by Dellivers et al.[12a] To understand the molecular structure of imidazopyrazinone derivatives systematically, we also analyzed the X-ray crystal structures of *N*-methyl derivatives **3** and **4** and evaluated their structural characteristics, accompanied by those of the protonated species of **1** and the neutral form of **2**. Table 1 summarizes the crystallographic data for **3** and **4**; their ORTEP drawings are shown in Fig. 1. In crystals of **3**, seven water molecules per two molecules of **3** were included as crystal waters. These water molecules made hydrogen-bonding interactions with **3**. In the case of **4**, there are two crystallographically independent molecules, **4(A)** and **4(B)**, in the asymmetric unit; **A** and **B** are described later. It is a noteworthy feature observed by X-ray crystal analyses of **3** and **4** that the core imidazopyrazinone rings of **3**, **4(A)**, and **4(B)** are virtually planar. The selected bond angles and the torsion angles for **3**, **4(A)**, and **4(B)** are summarized in Tables 2 and 3, respectively. The observed torsion angles for the imidazopyrazinone ring parts of **3**, **4(A)**, and **4(B)** are
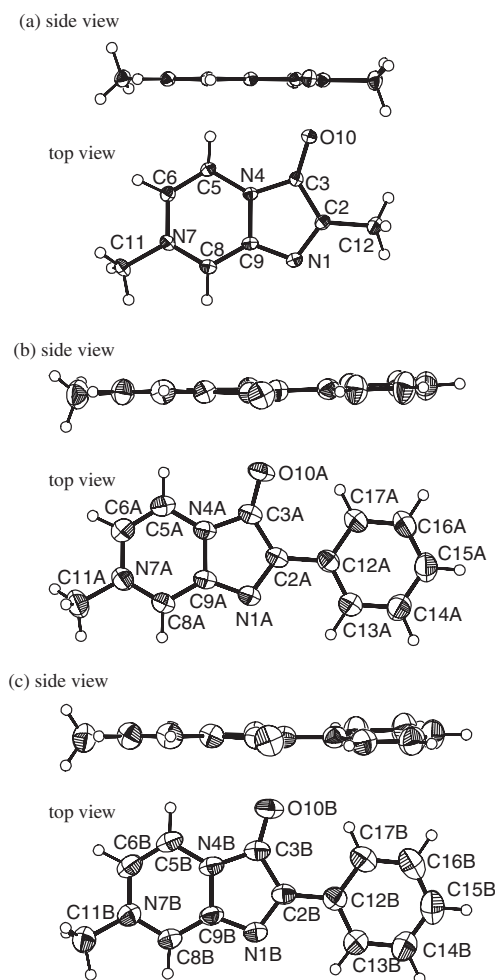
Results and Discussion

1. Preparation of Imidazopyrazinone Derivatives. Imidazopyrazinone derivatives **1** and **2** were prepared by a reported procedure.[12a,16,17] *N*-Methyl derivatives **3** and **4** were synthesized by the methylation of **1** and **2** with dimethyl sulfate or methyl iodide under basic conditions in a manner similar to the reported method.[13c] Under these conditions, the formation of the *O*-methyl product was negligible. On the other hand, the ethylation of **1** and **2** with ethyl iodide under basic condi-

Table 1. Crystal Date for **3** and **4**

	3	4
Empirical formula	$C_8H_9N_3O \cdot 3.5H_2O$	$C_{13}H_{11}N_3O$
FW	226.24	225.25
Temperature/K	110	295
Crystal system	Monoclinic	Triclinic
Space group	$C2/c$	$P\bar{1}$
a/Å	19.035(4)	12.2400(14)
b/Å	6.985(4)	12.9754(15)
c/Å	17.178(4)	8.2154(10)
α/°	90	103.868(10)
β/°	94.525(18)	98.147(11)
γ/°	90	116.258(8)
V/Å^3	2276.7(14)	1089.1(2)
Z	8	4
θ range for cell const./°	12.5–17.2	12.7–17.3
No. of reflections for cell const.	25	25
D_x/Mg m^{-3}	1.320	1.374
μ/mm^{-1}	0.108	0.091
$F(000)$	968	472
Crystal size/mm^3	$0.60 \times 0.30 \times 0.30$	$0.75 \times 0.18 \times 0.13$
θ range/°	2.15–27.50	2.66–27.50
Index ranges	$-24 \le h \le 24$, $0 \le k \le 9$, $-22 \le l \le 22$	$-15 \le h \le 15$, $-16 \le k \le 16$, $0 \le l \le 10$
Reflections collected	5513	5358
Independent reflections	2614 [R(int) = 0.0214]	5007 [R(int) = 0.0098]
Absorption correction	Ψ-scan	None
T_{max}, T_{min}	1.000, 0.967	—
Refinement method	Full-matrix least-squares on F^2	Full-matrix least-squares on F^2
No. of parameters	247	395
Goodness-of-fit on F^2	0.945	1.028
Final R indices [$I > 2\sigma(I)$]	$R1 = 0.0294$, $wR2 = 0.0842$	$R1 = 0.0405$, $wR2 = 0.1077$
R indices (all data)	$R1 = 0.0326$, $wR2 = 0.0877$	$R1 = 0.0525$, $wR2 = 0.1163$
Weighting Scheme	$1/[\sigma^2(F_o^2) + (0.061P)^2 + 0.1528P]$ where $P = (F_o^2 + 2F_c^2)/3$	$1/[\sigma^2(F_o^2) + (0.0585P)^2 + 0.9695P]$ where $P = (F_o^2 + 2F_c^2)/3$
$\Delta\rho_{max}$, $\Delta\rho_{min}$/e Å^{-3}	0.304, −0.271	0.177, −0.236

(a) side view

top view

(b) side view

top view

(c) side view

top view

Fig. 1.   ORTEP Drawings of **3** (a), **4(A)** (b), and **4(B)** (c).

Table 2.   Selected Bond Angles for **3** and **4**

	$\theta/°$		
	3·3.5H$_2$O	**4 (A)**	**4 (B)**
C(2)–N(1)–C(9)	106.16(7)	105.90(10)	106.02(10)
N(1)–C(2)–C(3)	112.02(8)	112.25(10)	111.91(11)
N(1)–C(2)–C(12)	122.86(8)	121.98(11)	121.99(11)
C(3)–C(2)–C(12)	125.12(8)	125.77(10)	126.08(12)
O(10)–C(3)–N(4)	124.91(8)	124.18(11)	124.52(12)
O(10)–C(3)–C(2)	131.83(8)	133.66(12)	132.92(13)
N(4)–C(3)–C(2)	103.25(7)	102.15(9)	102.56(10)
C(3)–N(4)–C(5)	131.91(7)	130.27(10)	131.09(11)
C(3)–N(4)–C(9)	108.35(7)	109.12(10)	108.78(10)
C(5)–N(4)–C(9)	119.74(7)	120.60(10)	120.09(11)
C(6)–C(5)–N(4)	118.67(8)	118.50(12)	118.37(12)
C(5)–C(6)–N(7)	121.45(8)	121.60(13)	122.21(13)
C(8)–N(7)–C(6)	120.42(8)	120.40(11)	119.78(12)
C(8)–N(7)–C(11)	120.40(8)	120.41(12)	120.82(12)
C(6)–N(7)–C(11)	119.18(8)	119.17(12)	119.39(12)
N(7)–C(8)–C(9)	120.11(8)	120.01(11)	120.32(12)
N(1)–C(9)–C(8)	130.18(8)	130.62(11)	130.07(12)
N(1)–C(9)–N(4)	110.22(8)	110.55(10)	110.70(11)
C(8)–C(9)–N(4)	119.61(8)	118.82(11)	119.21(11)

Scheme 1.

close to 0° or 180°, and the deviation of the torsion angles from 0° or 180° are below 3.5°, indicating the planarity of the core imidazopyrazinone ring. As a characteristic part of the imidazopyrazinone ring, we pay attention to the pyramidization of N7. The sums of the bond angles C6–N7–C8, C6–N7–C11, and C8–N7–C11 for **3**, **4(A)**, and **4(B)** are 360.00(14)°, 360.0(2)°, and 360.0(2)°, respectively, to show that the nitrogen atoms, N7, lie on the same plane with the carbon atoms C6, C8, and C11. In the case of **4(A)** and **4(B)**, 2-phenyl groups were almost co-planar with the imidazopyrazinone rings. The torsion angles N1–C2–C12–C13 of **4(A)** and **4(B)** are 0.21(18)° and 4.60(19)°, respectively, suggesting that a conjugated interaction between the imidazopyrazinone ring and the phenyl group prefers to a steric repulsion between O10 and the *ortho* phenyl protons.

The selected bond lengths of the imidazopyrazinone rings in **3**, **4(A)**, and **4(B)** are summarized in Table 4, accompanied by the reported data of **1** and **2**.[12a] The C3–O10 bond lengths of **2**, **3**, **4(A)**, and **4(B)** were observed as 1.259(3), 1.2642(11), 1.2464(14), and 1.2462(15) Å, respectively. These bond lengths are longer than the typical C=O bond length of a carbonyl compound, such as acetone (1.22 Å),[18] and are shorter than the C3–O10 bond length of the protonated molecule of **1** (1.313(4) Å). These values are similar to the C=O bond length of tropone **7** (1.26 Å), which has a zwitter-ionic nature in order

to have aromaticity.[19] Thus, these comparisons indicate that imidazopyrazinone derivatives have a weakened carbonyl character for the C3–O10 bond; the reason of these characteristic C3–O10 bond lengths is explained by the concept of aromaticity in a manner similar to tropone. An imidazopyrazinone ring (**I**) contains an antiaromatic 1,4-dihydropyrazine ring, and has 11 π-electrons, except for a π-electron on O10, as shown in Scheme 1. In order to increase the aromatic character, the zwitter-ionic structure **II**, which has a 10 π-electron ring and a single-bond character for the C3–O10 bond, would contribute in the resonance structures. Then, imidazopyrazinone derivatives showed a weakened carbonyl character for the C3–O10 bond.

In the partial pyrazine rings of **2**, **3**, **4(A)**, and **4(B)**, the N4–C5 and C6–N7 bonds were in the range of 1.37–1.39 Å, and the C5–C6 bonds were in the range of 1.33–1.35 Å. These bond lengths were evaluated by comparing with reference compounds, pyrazine (**8**), which has "aromatic" character, and a 1,4-dihydropyrazine derivative (**9a**), which has "anti-aromatic" character.[20,21] Pyrazine **8** possesses C–N and C–C bonds of 1.34 and 1.40 Å lengths, respectively,[22] and **9a** possesses C–N and C–C bonds of 1.42 and 1.32 Å lengths in a planar ring, respectively.[23] The C–N and C–C bonds of the partial pyrazine rings of **2**–**4** are of intermediate lengths between those of **8** and **9a**, suggesting that the imidazopyrazinone rings of **2**–**4** possess

Table 3. Selected Torsion Angles for **3** and **4**

	$\theta/°$		
	3·3.5H$_2$O	**4 (A)**	**4 (B)**
C(9)–N(1)–C(2)–C(3)	−0.12(10)	0.62(13)	−0.24(15)
C(9)–N(1)–C(2)–C(12)	−179.95(8)	−178.84(11)	−178.68(11)
N(1)–C(2)–C(3)–O(10)	−178.99(9)	178.32(13)	179.30(14)
C(12)–C(2)–C(3)–O(10)	0.84(15)	−2.2(2)	−2.3(2)
N(1)–C(2)–C(3)–N(4)	0.25(9)	−1.23(13)	−0.90(14)
C(12)–C(2)–C(3)–N(4)	−179.92(8)	178.20(11)	177.46(11)
O(10)–C(3)–N(4)–C(5)	−1.81(14)	2.6(2)	−1.0(2)
C(2)–C(3)–N(4)–C(5)	178.88(8)	−177.82(12)	179.22(13)
O(10)–C(3)–N(4)–C(9)	179.03(8)	−178.29(11)	−178.54(12)
C(2)–C(3)–N(4)–C(9)	−0.27(9)	1.32(12)	1.64(13)
C(3)–N(4)–C(5)–C(6)	−179.64(8)	−178.50(12)	−176.38(13)
C(9)–N(4)–C(5)–C(6)	−0.56(12)	2.45(18)	1.0(2)
N(4)–C(5)–C(6)–N(7)	0.03(12)	−0.4(2)	0.4(2)
C(5)–C(6)–N(7)–C(8)	0.33(13)	−1.6(2)	−1.4(2)
C(5)–C(6)–N(7)–C(11)	−179.39(8)	177.00(14)	177.03(14)
C(6)–N(7)–C(8)–C(9)	−0.14(13)	1.38(19)	1.0(2)
C(11)–N(7)–C(8)–C(9)	179.58(8)	−177.15(13)	−177.47(14)
C(2)–N(1)–C(9)–C(8)	−179.84(9)	−178.87(13)	−176.92(14)
C(2)–N(1)–C(9)–N(4)	−0.06(10)	0.26(13)	1.31(14)
N(7)–C(8)–C(9)–N(1)	179.36(8)	179.71(12)	178.51(14)
N(7)–C(8)–C(9)–N(4)	−0.40(13)	0.65(18)	0.4(2)
C(3)–N(4)–C(9)–N(1)	0.22(10)	−1.07(13)	−1.96(15)
C(5)–N(4)–C(9)–N(1)	−179.05(7)	178.16(11)	−179.85(12)
C(3)–N(4)–C(9)–C(8)	−179.97(7)	178.17(11)	176.49(12)
C(5)–N(4)–C(9)–C(8)	0.76(12)	−2.60(17)	−1.41(19)
N(1)–C(2)–C(12)–C(13)	—	0.21(18)	4.60(19)

Table 4. Selected Bond Lengths for **1**–**4**

	$l/Å$				
	1 + HCl (Ref. 12a)	**2·2H$_2$O** (Ref. 12a)	**3·3.5H$_2$O** (This work)	**4 (A)**	**4 (B)**
				(This work)	
N(1)–C(2)	1.342(4)	1.344(3)	1.3396(12)	1.3485(14)	1.3499(16)
N(1)–C(9)	1.342(4)	1.345(5)	1.3485(12)	1.3410(16)	1.3378(16)
C(2)–C(3)	1.407(4)	1.444(4)	1.4432(12)	1.4542(17)	1.4535(17)
C(2)–C(12)	1.488(4)	1.461(3)	1.4902(13)	1.4622(17)	1.4593(19)
C(3)–O(10)	1.313(4)	1.259(3)	1.2642(11)	1.2464(14)	1.2462(15)
C(3)–N(4)	1.340(4)	1.366(3)	1.3737(11)	1.3778(16)	1.3755(17)
N(4)–C(5)	1.388(4)	1.392(3)	1.3922(11)	1.3810(17)	1.3855(17)
N(4)–C(9)	1.397(4)	1.402(3)	1.4093(11)	1.4050(14)	1.4069(15)
C(5)–C(6)	1.328(5)	1.333(4)	1.3457(13)	1.335(2)	1.331(2)
C(6)–N(7)	1.369(4)	1.374(3)	1.3921(12)	1.3885(17)	1.3901(18)
N(7)–C(8)	1.336(4)	1.345(3)	1.3459(12)	1.3458(17)	1.3443(17)
N(7)–C(11)	1.365(5)	1.352(3)	1.4716(11)	1.4654(17)	1.4660(19)
C(8)–C(9)	—	—	1.3681(13)	1.3710(17)	1.3644(19)

small portions of aromatic character by a resonance effect, as shown in Scheme 1, with a decreasing "anti-aromatic" property of the partial 1,4-dihydropyrazine parts. As another characteristics, the C2–C3 bonds in the partial imidazolone rings were the longest (1.44–1.45 Å) in the imidazopyrazinone ring systems.

3. Intermolecular Interactions in Crystals. In single crystals of **3** and **4**, molecules are oriented in a characteristic pattern. In the case of **3**, single crystals contain crystal water molecules, and the arrangement of **3** makes a column structure
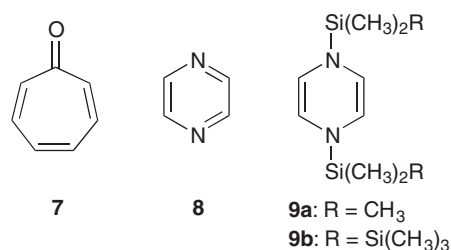
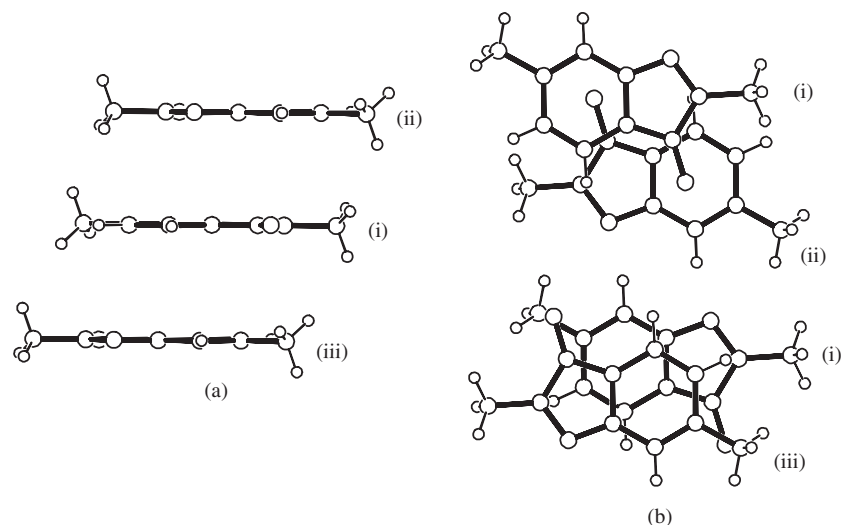**7**　　**8**　　**9a**: R = CH$_3$
　　　　　　　　9b: R = Si(CH$_3$)$_3$

Chart 2.

Fig. 2. (a) Column arrangement of **3**. (b) Two parallel pairs in the column arrangement. Symmetry code: (i) *x*, *y*, *z*; (ii) $1/2 - x$, $-1/2 - y$, $1 - z$; (iii) $1/2 - x$, $1/2 - y$, $1 - z$.

with a π–π stacking interaction, as shown in Fig. 2. A side-view of the column arrangement shows that molecules of **3** have two types of face-to-face interactions and are aligned in parallel to each other. The face-to-face distances (interplane distances) are 3.234(4) Å between molecules (i) and (ii), and 3.270(3) Å between molecules (i) and (iii), where (i) to (iii) are symmetry codes defined in Fig. 2; these face-to-face distances are close to a typical van der Waals contact. The top-view in Fig. 2 indicates that molecule (i) overlaps with the neighboring molecules (ii) and (iii) in a column arrangement. The arrangement pattern is a head-to-tail alternation, and a neighboring molecule in the column arrangement turns 180° from the other. The π–π stacking column structures may be stabilized by dipole–dipole interactions between neighboring molecules,

since **3** has a polarized character originated by the zwitter-ionic resonance structure **II**. The intermolecular hydrogen bonds in **3** and **4** are summarized in Table 5. The arrangement of **3** and water molecules is displayed in Fig. 3, which shows that four column structures are connected by water molecules. Between the columns, molecules of **3** make hydrogen-bonding interactions with water molecules at N1 and O10. It is noteworthy that in the hydrogen-bonding interactions, molecules of **3** act as a hydrogen-bond acceptor, and water molecules act as a hydrogen-bond donor. This behavior of **3** to make a hydrogen-bonding network in a crystal is similar to that of **2** reported by Dellivers et al.[12a] Thus, an imidazopyrazinone derivative has an ability to make hydrogen-bonds at N1 and O10 as a hydrogen-bond acceptor with a hydrogen-bond donor molecule, such

Table 5. Hydrogen Bonds for **3** and **4**

D–H···A	$d_{(H\cdots A)}$/Å	$d_{(D\cdots A)}$/Å	$\angle(DHA)$/°
3			
O(2)–H(21)···N(1)	1.970(16)	2.8212(12)	163.4(14)
O(2)–H(22)···O(5)	1.85(4)	2.7526(12)	172(3)
O(2)–H(23)···O(3)[i]	1.94(3)	2.7636(14)	166(3)
O(3)–H(31)···O(10)	1.879(17)	2.7696(11)	173.3(15)
O(3)–H(32)···O(2)[i]	1.96(3)	2.7636(14)	168(3)
O(3)–H(33)···O(4)[ii]	1.93(3)	2.7386(14)	174(3)
O(4)–H(41)···O(10)	1.892(17)	2.7490(11)	171.9(13)
O(4)–H(42)···O(5)[iii]	1.99(3)	2.7419(11)	172(3)
O(4)–H(43)···O(3)[ii]	1.87(3)	2.7386(14)	171(3)
O(5)–H(51)···O(2)	1.90(3)	2.7526(12)	176(3)
O(5)–H(52)···O(4)[iv]	1.92(3)	2.7419(11)	168(3)
4			
C(8A)–H(8A)···O(10B)	2.331(15)	3.2348(16)	154.0(12)
C(11A)–H(1A)···O(10B)	2.45(2)	3.339(2)	149.9(17)
C(5A)–H(5A)···N(1B)[v]	2.461(16)	3.3560(17)	155.8(12)
C(5B)–H(5B)···O(10A)[vi]	2.403(16)	3.1726(16)	135.5(12)
C(11B)–H(1B)···N(1A)[vii]	2.54(2)	3.483(2)	153.2(15)
C(8B)–H(8B)···N(1A)[vii]	2.567(16)	3.4254(17)	145.2(12)

Symmetry codes: i) $-x + 1/2$, $-y - 1/2$, $-z + 1$; ii) $-x$, $-y$, $-z + 1$; iii) $x - 1/2$, $y - 1/2$, z; iv) $-x + 1/2$, $y + 1/2$, $-z + 1/2$; v) $x - 1$, y, z; vi) $-x$, $-y + 1$, $-z + 1$; vii) $-x + 1$, $-y + 1$, $-z + 1$.
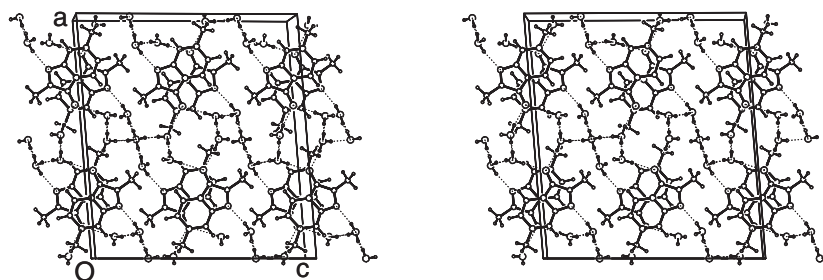
Fig. 3. Crystal structure of **3** viewed along the *b* axis. Dotted lines indicate intermolecular hydrogen bonds.
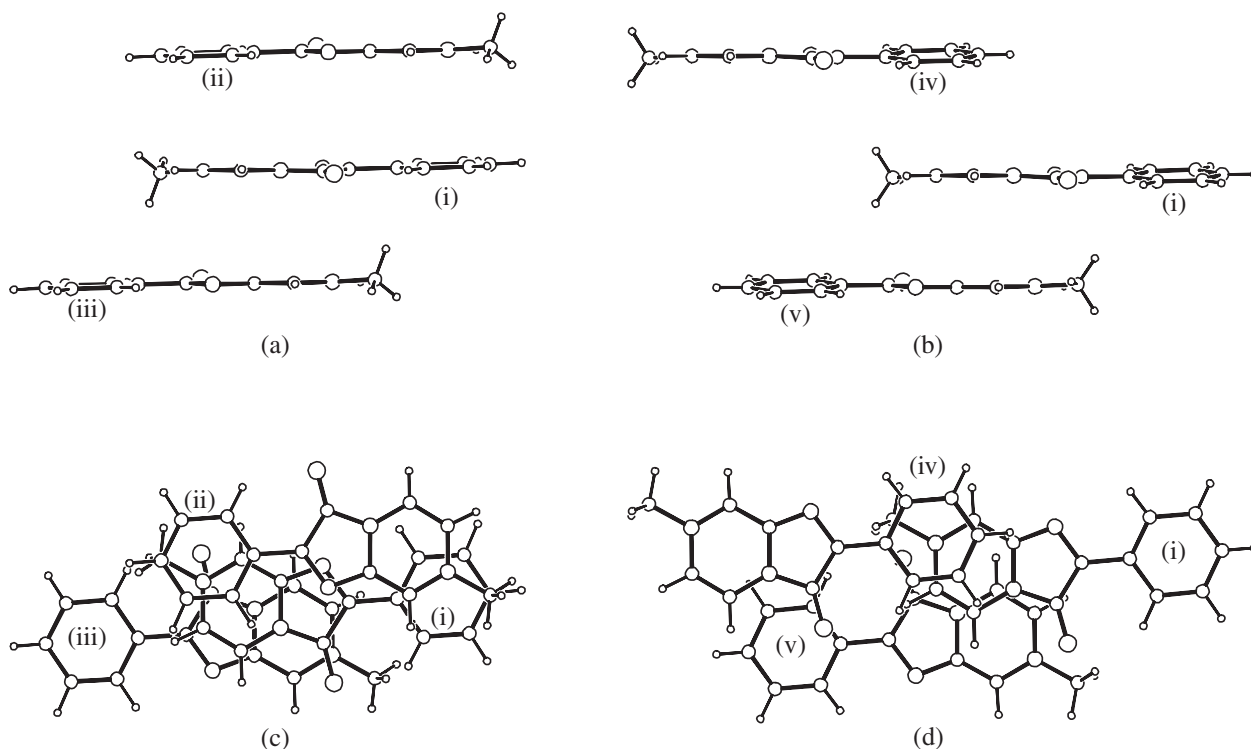

Fig. 4. (a), (b) Side view of column arrangement of **4(A)** and **4(B)**, respectively. (c), (d) Top view for **4(A)** and **4(B)**, respectively. Symmetry code: (i) *x*, *y*, *z*; (ii) −*x*, 1 − *y*, −*z*; (iii) −*x*, 1 − *y*, 1 − *z*; (iv) *x*, *y*, 1 + *z*; (v) 1 − *x*, 1 − *y*, 1 − *z*.

as a water molecule. Major water molecules connect the column structures of **3**, and water molecules placed in the center of four column structures interact with only water molecules by hydrogen-bonding interactions. These water molecules also make a column structure, and are interesting as an example of a water-cluster in the crystalline state.[24]

In crystals of **4**, there are two π–π stacking column structures, **A** and **B**, as shown in Fig. 4. Side-views of the column structures of **A** and **B** show that molecules have a π–π stacking interaction and are aligned parallel to each other. In the column structure **A**, the arrangements of the molecules are a head-to-tail alternation pattern. The interplane distances are 3.544(3) Å for molecules (i) and (ii) and 3.380(3) Å for (i) and (iii), where (i) to (iii) are symmetry codes defined in Fig. 4. One pair of molecules, (i) and (iv), in the column structure **B** has a head-to-head arrangement with an interplane distance of 3.543(3) Å, while another pair, (i) and (v), has a head-to-tail arrangement with a distance of 3.301(3) Å. The degree of overlap of the molecules in column **A** is larger than that in column **B**. Thus,

the π–π stacking interaction stabilizes the column structure in the crystals by dipole–dipole interactions in a manner similar to that of **3**. The relative arrangements of the two column structures are illustrated in Fig. 5. Column structures **A** and **B** are aligned perpendicular to each other, causing the pyrazine parts of the molecules in each column to be closely placed. Two columns are linked by the intermolecular CH···O and CH···N hydrogen bonds summarized in Table 5.

4. UV/Vis Absorption Spectra.   (a) Solvatochromic Property of Imidazopyrazinone Derivatives 1-4: Imidazopyrazinone derivatives **1**–**4** were colored compounds. 2-Methyl derivatives **1** and **3** showed a yellowish color, and the brightness of their solutions was changed depending upon the solvent; in the case of 2-phenyl derivatives **2** and **4**, the color of solutions varied from orange to red depending upon the solvent (Fig. 6). The color change of solutions of **1** was found by the Cormier group[14] and the origin of this color change was suggested to be a hydrogen-bonding interaction. To establish the solvatochromic character of imidazopyrazinone derivatives,
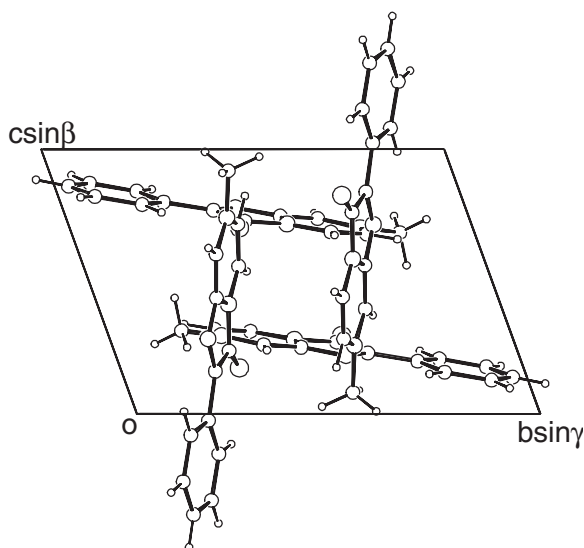
Fig. 5. Crystal structure of **4** viewed along the *a* axis.
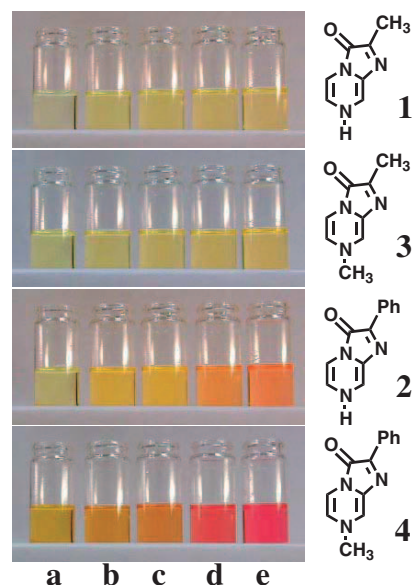
Fig. 6. Illustration of solvatochromism of **1–4**. Dilute solutions of **1–4** in various solvents; (a) water, (b) methanol, (c) 2-propanol, (d) acetonitrile, and (e) DMSO.
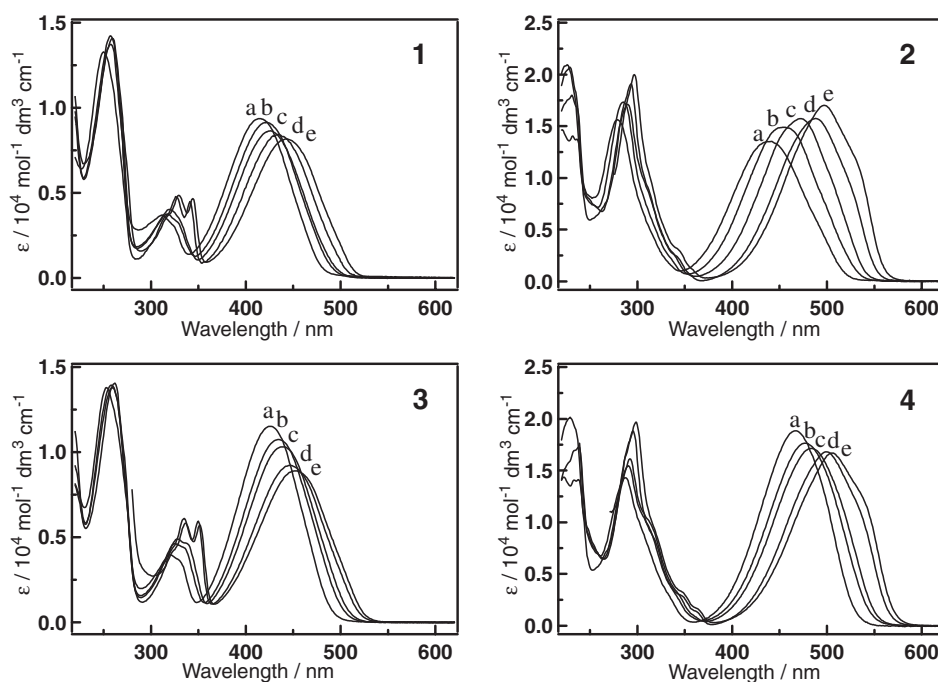
Fig. 7. UV/vis absorption spectra of **1–4** in various solvents; (a) water, (b) methanol, (c) 2-propanol, (d) acetonitrile, and (e) DMSO.

we systematically investigated the UV/vis absorption spectra of **1–4** in various solvents. Because of a low solubility of **1–4** in nonpolar solvents, such as hexane and chloroform, we measured the UV/vis absorption spectra of **1–4** in polar solvents: DMSO, acetonitrile, 2-propanol, methanol, and water. The UV/vis absorption spectra of **1–4** (Fig. 7) showed a characteristic spectral change dependent upon the solvent changes. The absorption maxima and molar absorption coefficients of **1–4** are summarized in Table 6 accompanied by those of **5** and **6**. For **1–4**, the lowest energy band of each compound showed the shortest wavelength in water and the longest wavelength in

DMSO. To clarify the origin of this solvatochromic property, the wavenumbers (E_a (cm^{-1})) of the lowest energy bands were correlated to various solvent parameters,[25] and it was found that the E_a values were linearly correlated to the Kamlet–Taft's solvatochromic parameter (α) values,[26] as shown in Fig. 8. On the other hand, the Kamlet–Taft's β and π^* values[26] did not show any correlation with E_a. This result indicates that a hydrogen-bonding interaction of an imidazopyrazinone derivative with solvent molecules specifically works for the solvatochromism. In the hydrogen-bonding interaction, a hydrogen-bond donor part of solvent molecules interacts with a hydrogen-bond ac-
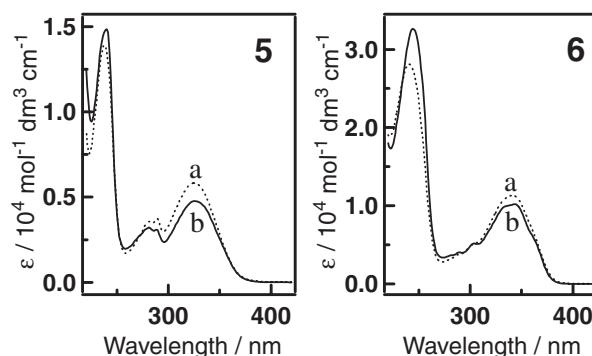
Table 6. UV/Vis Absorption Data of **1–6** in Various Solvents

Solvents (α-value[a])	λ_{max}/nm ($\varepsilon/10^4$ dm^3 mol^{-1} cm^{-1})					
	1	**2**	**3**	**4**	**5**	**6**
DMSO	442 (0.82)	497 (1.70)	452 (0.89)	505 (1.67)	328 (0.49)	345 (1.05)
(0.00)	344 (0.47)	297 (2.00)	351 (0.57)	299 (1.97)	290 (0.34)	306 (0.56)
	329 (0.48)		336 (0.58)		282 (0.36)	291 (0.44)
						283 (0.41)
Acetonitrile	434 (0.84)	488 (1.57)	448 (0.92)	499 (1.68)	325 (0.48)	343 (1.02)
(0.19)	341 (0.45)	293 (1.91)	350 (0.60)	295 (1.88)	288 (0.31)	304 (0.52)
	326 (0.48)	236 (1.37)	335 (0.61)	238 (1.41)	281 (0.32)	289 (0.40)
	250 (1.33)	232 (1.40)	253 (1.38)	233 (1.41)	240 (1.49)	281 (0.37)
						244 (3.26)
2-Propanol	426 (0.86)	472 (1.57)	438 (1.03)	483 (1.71)	327 (0.54)	344 (1.11)
(0.76)	319 (0.40)	290 (1.71)	328 (0.49)	292 (1.61)	289 (0.34)	242 (3.06)
	259 (1.41)	231 (1.80)	258 (1.39)	238 (1.73)	282 (0.34)	
					239 (1.51)	
Methanol	422 (0.91)	454 (1.49)	434 (1.07)	476 (1.76)	328 (0.56)	343 (1.12)
(0.93)	317 (0.38)	285 (1.73)	325 (0.46)	290 (1.55)	289 (0.35)	241 (3.01)
	257 (1.42)	229 (2.07)	259 (1.38)		282 (0.35)	
					239 (1.52)	
Water	414 (0.94)	442 (1.35)	426 (1.15)	467 (1.88)	325 (0.58)	341 (1.13)
(1.17)	311 (0.37)	279 (1.56)	320 (0.40)	287 (1.43)	289 (0.38)	240 (2.81)
	257 (1.37)	226 (2.09)	262 (1.41)	229 (2.02)	282 (0.36)	
					237 (1.39)	

a) Ref. 26.
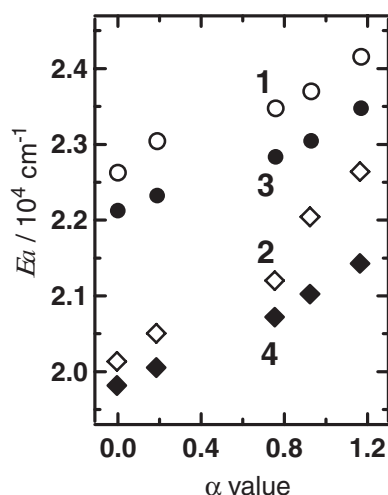
Fig. 8. Plots of wavenumbers E_a (cm^{-1}) of the lowest energy bands for **1–4** against the Kamlet–Taft's α values.

Fig. 9. UV/vis absorption spectra of **5** and **6** in water (a) and acetonitrile (b).

ceptor part of an imidazopyrazinone derivative for changing the energy levels of frontier orbitals of the imidazopyrazinone π-system. Figure 8 also shows that the slopes of the linear lines of **1–4** are similar to each other, indicating that solvent molecules interact with molecules of **1–4** by hydrogen bonding with a similar tendency. These similarities of the UV/vis absorption property among **1–4** indicates that **1–4** possess a common π-electronic character. The difference in the absorption maxima among **1–4** in a particular solvent is evaluated as a perturbative substituent effect on the electronic property of the imidazopyrazinone π-system. A replacement of the methyl group at C2 in **1** or **3** by a phenyl group, which gives **2** or **4**, results in a bathochromic shift of the lowest energy band by more than 30 nm.

N-Methylation of **1** or **2**, which gives **3** or **4**, results in a shift of the lowest energy band to ca. 10 nm longer wavelength. These spectral shifts, caused by phenyl substitution at C2 and methylation at N7, are well correlated to changes of the calculated HOMO–LUMO energy gaps, described later, indicating that these substituent effects on the spectral characteristics can be systematically explained by a small change in the π-electronic property.

(b) *O*-Alkylated Derivatives: *O*-Ethyl derivatives **5** and **6** showed absorption maxima at around 325 and 340 nm in various solvents, respectively (Fig. 9), and **5** and **6** showed only small spectral changes dependent upon the solvent change (Table 6). These spectroscopic characteristics of **5** and **6** are different from those of **1–4**, indicating that the π-systems of **5** and **6** have quite different properties from those of **1–4**. N–H derivatives **1** and **2** have a possibility to make several tautomeric structures, as suggested by Goto.[13c,d] Based on these previous reports, we focus on a tautomeric equilibrium between
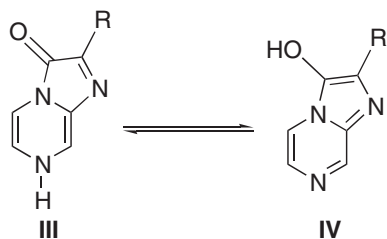
Scheme 2.

the NH form (**III**) and the OH form (**IV**) in a solution (Scheme 2). The evidence that the absorption spectral behavior of **1** and **2** was similar to that of *N*-methyl derivatives **3** and **4**, and was different from that of **5** and **6**, clearly indicates that **1** and **2** are preferable to be the **III** form in tautomeric equilibrium in solutions, and that a contribution of the **IV** form is negligible. This conclusion matches the conclusion of Goto's reports, in which the spectral properties of **1** were compared to those of **3** and 3-aminoimidazo[1,2-*a*]pyrazine derivatives.[13d]

(c) Effects of the Addition of an Acid: It has been well studied that the UV/vis absorption spectra of imidazopyrazinone derivatives were changed by the addition of an acid to their solutions.[13d,14,15] These spectral changes are caused by the generation of a protonated species. Since there is no quantitative research on the formation of a protonated species, we systematically reinvestigated the UV/vis absorption spectra of **1–6** in the presence of an acid. In this study, we used methanesulfonic acid (MSA) as an acid. In the presence of MSA in DMSO and methanol at 25 °C, protonated species of **1–6** showed the characteristic UV/vis absorption spectra. By adding MSA to a solution of **1** in DMSO, the peaks at 442, 344, and 329 nm decreased along with an increase of the peak at 382 nm, and the isosbestic points were observed at 407, 346, and 304 nm, as shown in Fig. 10. In addition to the major peaks, a weak shoulder absorption band was observed at around 470 nm, suggesting the generation of a minor protonated species. Similar spectral changes were also observed for the protonation of **2** in DMSO in the presence of MSA (Fig. 10). In the case of **2**, two clear peaks at 517 and 405 nm increased upon the addition of MSA, suggesting the generation of two protonated species. The existence of two protonated species of **2** was supported by a measurement of the fluorescence spectra, in which excitation at 405 and 517 nm resulted in fluorescence emissions with the maxima at 563 and 583 nm, respectively.

These spectral changes, caused by the formation of protonated species, were evaluated using the Eq. 1, where an imidazopyrazinone derivative (**IP**) and MSA (**A–H**) make an equilibrium with protonated species ((**IP + H**)$^+$) and a methanesulfonate anion (**A**$^-$).

$$\mathbf{IP} + \mathbf{A\text{–}H} \overset{K}{\rightleftharpoons} (\mathbf{IP} + \mathbf{H})^+ + \mathbf{A}^- \tag{1}$$

Since the spectral changes in Fig. 10 showed clear isosbestic points, the formation of two protonated species would occur at the same time as competitive processes. Thus, the formation constants (*K*) of the protonated species for **1** and **2** were estimated as a summation of the formation constants (*K*) for two protonated species. To estimate the *K* values, the spectral changes in Fig. 10 were analyzed by Eq. 2.[27] The value A_0 is the absorbance of an imidazopyrazinone derivative (**IP**) at a
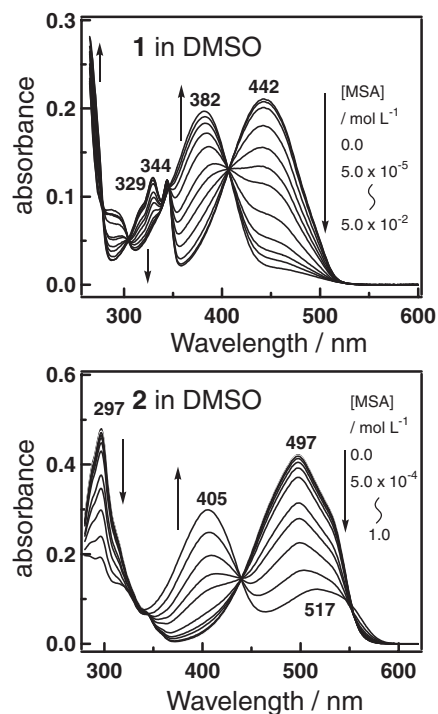

Fig. 10. UV/vis absorption spectra of **1** (2.6×10^{-5} mol L^{-1}) and **2** (2.5×10^{-5} mol L^{-1}) in DMSO containing various concentrations of methanesulfonic acid at 25 ± 1 °C.

chosen wavelength in the absence of MSA. After the addition of MSA, the absorbance at the chosen wavelength is observed as A_{obs}. The difference between A_{obs} and A_0 is given by

$$\begin{aligned} A_{obs} - A_0 = 0.5\Delta\varepsilon([IP]_t + [MSA]_t + 1/K - \{([IP]_t \\ + [MSA]_t + 1/K)^2 - 4[IP]_t[MSA]_t\}^{1/2}), \end{aligned} \tag{2}$$

where $[IP]_t$ and $[MSA]_t$ are the initial concentrations of **IP** and MSA, respectively, and $\Delta\varepsilon$ is the difference in the molar absorptivity between **IP** and its protonated species, $(\mathbf{IP} + \mathbf{H})^+$, at a chosen wavelength. The $(A_{obs} - A_0)$ values were plotted against the $[MSA]_t$ values, as shown in Fig. 11. The data were analyzed by a nonlinear least-squares curve fitting for Eq. 2, and the *K* values for protonation of **1** and **2** in DMSO were obtained as 383 ± 5 and 15.3 ± 0.7, respectively. The $\Delta\varepsilon$ values at 442 nm for **1** and at 497 nm for **2** were also estimated as -7620 ± 30 and -13400 ± 200, respectively. It is one of
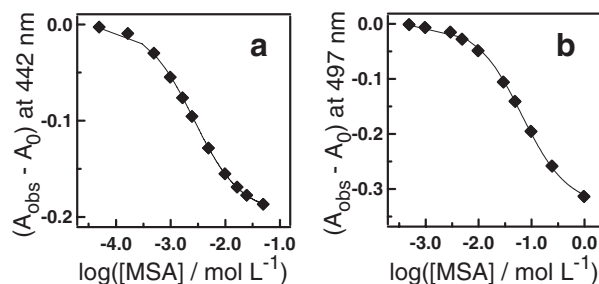

Fig. 11. Plot of $(A_{obs} - A_0)$ at 442 nm vs [MSA] for protonation of **1** (**a**) and plot of $(A_{obs} - A_0)$ at 497 nm vs [MSA] for protonation of **2** (**b**) in DMSO at 25 ± 1 °C. The solid lines correspond to the fitted curve to Eq. 2.
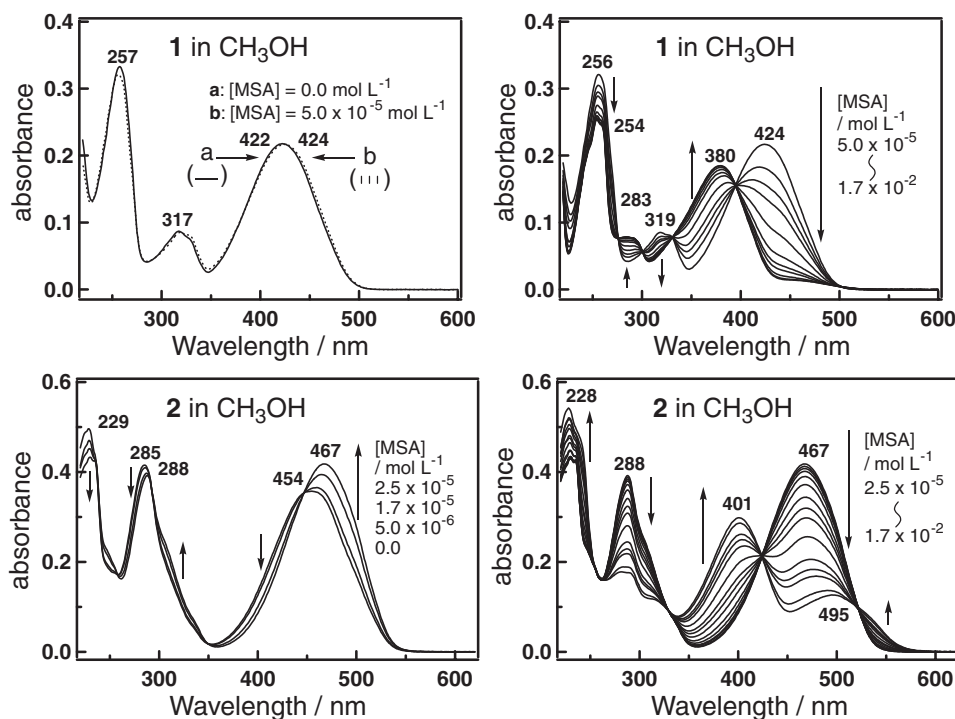
Fig. 12.   UV/vis absorption spectra of **1** (2.4×10^{-5} mol L^{-1}) and **2** (2.4×10^{-5} mol L^{-1}) in methanol containing various concentrations of methanesulfonic acid at 25 ± 1 °C.

the characteristics that the K value for the protonation of **1** is larger than that for the protonation of **2**.

In the presence of MSA in methanol, the UV/vis absorption spectra of **1** and **2** showed the stepwise changes shown in Fig. 12. In the case of **1**, a small spectral shift was observed in the presence of MSA at 5.0×10^{-5} mol L^{-1}. After the addition of MSA, more than 5.0×10^{-5} mol L^{-1}, the growth of the clear peaks at 380 and 283 nm was observed as the second spectral change with the isosbestic points in a manner similar to those in DMSO. In the case of **2**, the addition of MSA less than 2.5×10^{-5} mol L^{-1} increased the absorption band at 467 nm with the isosbestic points at 446, 292, and 239 nm. After the addition of MSA, by more than 2.5×10^{-5} mol L^{-1}, two peaks at 495 and 401 nm increased with a decrease of the peak at 467 nm. The second spectral change also showed clear isosbestic points at 424, 328, and 254 nm in a manner similar to those in DMSO. These observations of the first-step spectral changes by adding a low concentration of MSA are particular to the spectral changes of **1** and **2** in methanol. No first-step spectral change of **1** and **2** was observed in DMSO in the presence of MSA, and alkylated derivatives **3–6** also showed only one spectral change in DMSO and methanol in the presence of MSA, as described below. Thus, the N–H moiety of **1** and **2** may have an interaction with methanol molecules, and this interaction is lost by the addition of a low concentration of MSA, resulting in a first-step spectral change. The nature of this interaction may have a hydrogen-bonding interaction. The second-step spectral changes of **1** and **2** in methanol are similar to the spectral change observed in DMSO (Fig. 10). Two protonated species of **1** showed absorption maxima at 380 and ca. 460 nm, respectively, and those of **2** showed clear absorption maxima at 495 and 401 nm, respectively. The proportions of two absorption

bands for the two protonated species of **1** or **2** in DMSO and methanol were close to each other. It is noteworthy that the red-shifted lowest energy band showed a characteristic solvent-dependent spectral shift, although the blue-shifted lowest energy band showed a negligible solvent-dependent spectral shift. Especially, the absorption maxima of a protonated species of **2** shifted from 517 nm in DMSO to 495 nm in methanol. This spectral change, in which the absorption maximum was shifted to higher energy region in a protic solvent, is similar to the solvatochromic character of neutral molecules of **1–4**. This result suggests that protonated species possessing the red-shifted lowest energy band has a π-electronic system similar to those of neutral molecules of **1–4**. The second-step spectral changes of **1** and **2** observed by adding MSA in methanol were evaluated as the protonation process of Eq. 1. Data analyses using Eq. 2 gave the K values for the protonation of **1** and **2** as 3140 ± 160 and 519 ± 8, respectively. The $\Delta\varepsilon$ values at 422 nm for **1** and at 497 nm for **2** were also estimated as -7790 ± 80 and -14700 ± 70, respectively.

Spectral changes caused by the formation of protonated species of alkylated derivatives **3–6** in DMSO and methanol containing MSA are illustrated in Figs. 13 and 14. All derivatives gave spectral changes with clear isosbestic points; these spectral changes were analyzed as the protonation processes of Eq. 1 quantitatively. The formation constants (K) for the protonations were estimated by a nonlinear least-squares curve fitting with Eq. 2. Table 7 summarizes the K values and the absorption maxima of the protonated species. *N*-Methyl derivatives **3** and **4** showed similar spectral changes to those of **1** and **2** (Fig. 13). In the case of the protonation of **3**, the major protonated species had absorption maxima at 388 and 386 nm in DMSO and methanol, respectively, and the minor protonated
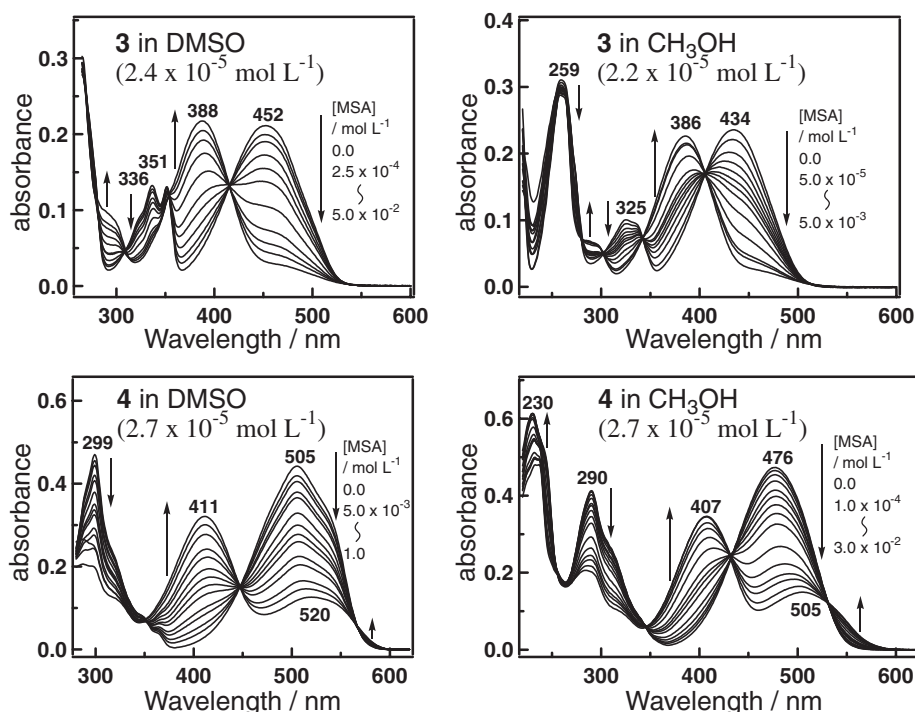
S. Nakai et al.

Bull. Chem. Soc. Jpn., 76, No. 12 (2003) 2371

Fig. 13.   UV/vis absorption spectra of **3** and **4** in DMSO and methanol containing various concentrations of methanesulfonic acid at 25 ± 1 °C.
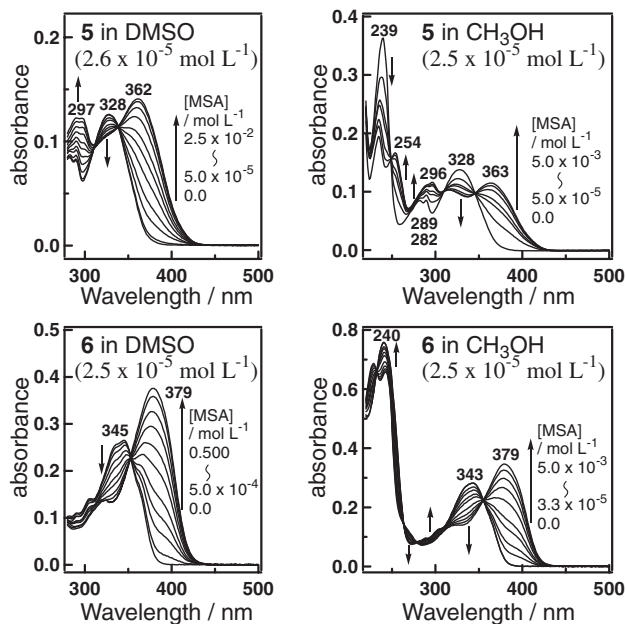

Fig. 14.   UV/vis absorption spectra of **5** and **6** in DMSO and methanol containing various concentrations of methanesulfonic acid at 25 ± 1 °C.

species showed a shoulder absorption band at around 460–470 nm. In the case of two protonated species of **4**, one showed absorption maxima at 411 and 407 nm in DMSO and methanol, respectively, and another showed absorption maxima at 520 and 505 nm in DMSO and methanol, respectively. As an effect of methylation at N7, the absorption maxima of two protonated species of **3** or **4** were shifted to a lower energy region from

those of the corresponding protonated species of the N–H derivatives, **1** or **2**. The K values for the protonation of **3** and **4** in DMSO and methanol were smaller than those for the protonation of **1** and **2** in DMSO and methanol, respectively (Table 7).
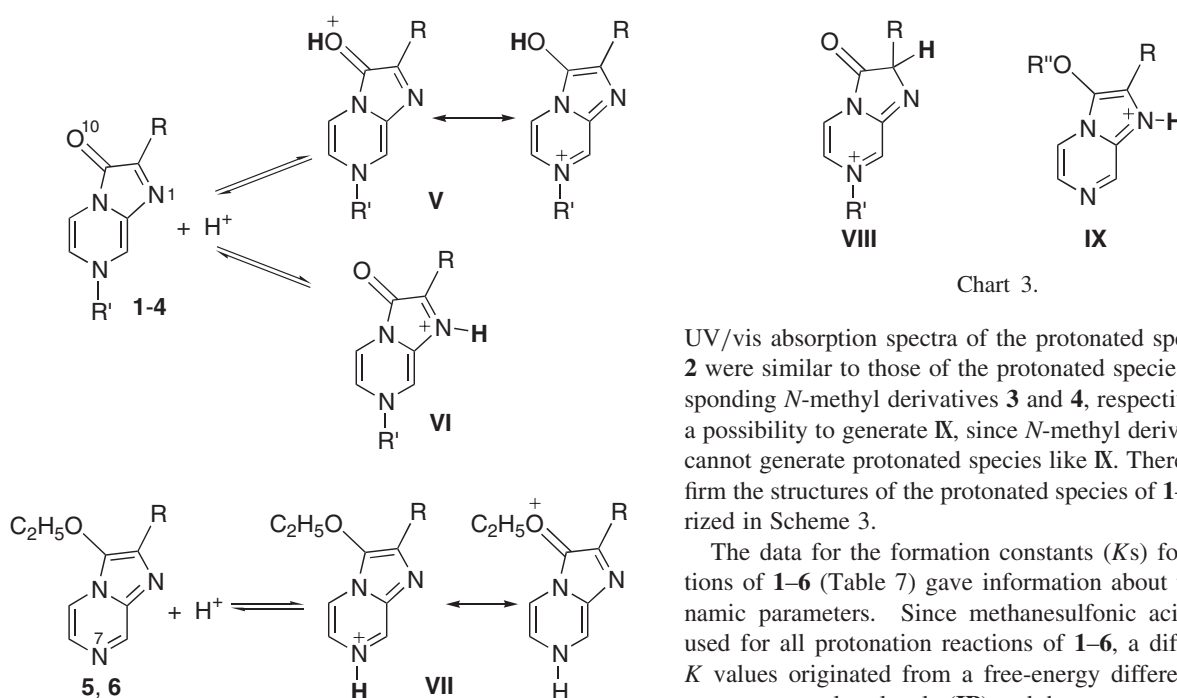
Protonated species of **5** and **6** showed a red-shifted lowest energy band compared to the neutral species in DMSO and methanol in the presence of MSA (Fig. 14). The absorption maxima of the protonated species of **5** were observed at 362 and 363 nm in DMSO and methanol, respectively, and the absorption maxima of protonated species of **6** were observed at 379 nm in DMSO and methanol. It is obvious that the protonated species of **5** and **6** have no solvatochromic property. The K values for the protonation of **5** in DMSO and methanol were larger than those for the protonation of **1** and **3** (Table 7). Similarly, the K values for the protonation of **6** in DMSO and methanol were larger than those for the protonation of **2** and **4**.

Based on reports of the Goto group,[13d] the spectroscopic data were assigned to specific protonated structures (Scheme 3). It was reported that the protonated species of **1** and **3** in methanol containing HCl showed blue-shifted absorption maxima at 380 and 387 nm, respectively. Our data reproduced their observation. The structures of the protonated species of **1** and **3** in methanol have been assigned to the *O*-protonated structure **V**. In aqueous HCl solutions, **1** and **3** gave protonated species with red-shifted absorption maxima at 440 and 445 nm, respectively. The structures of this protonated species were assigned to the *N*-protonated structure **VI**. Thus, the major protonated species of **1** and **3**, which have blue-shifted lowest energy bands in DMSO and methanol, are assigned to structure **V** and the minor protonated species, which have red-shifted lowest energy bands, are assigned to structure **VI**. The participation of the major protonated species **V** for **1** is also supported by an X-ray crystallographic analysis of the HCl salt of **1**.[12a] Similarly,

Table 7. Absorption Maxima $\lambda_{\max}$ and Formation Constants K for Protonated Species of **1–6** in DMSO and Methanol Containing Methanesulfonic Acid at 25 ± 1 °C

Compound	In DMSO		In methanol	
	$\lambda_{\max}$ (IP + H)$^+$/nm	K/mol^{-1} L	$\lambda_{\max}$ (IP + H)$^+$/nm	K/mol^{-1} L
1	470 (sh)$^{a)}$	383 ± 5	460 (sh)$^{a)}$	3140 ± 160
	382		380	
2	517	15.3 ± 0.7	495	519 ± 8
	405		401	
3	470 (sh)$^{a)}$	247 ± 2	460 (sh)$^{a)}$	2380 ± 100
	388		386	
4	520	9.11 ± 0.48	505	364 ± 9
	411		407	
5	362	735 ± 10	363	20600 ± 4500
6	379	118 ± 4	379	7540 ± 910

a) Shoulder peak.

Scheme 3.

Chart 3.

two protonated species of **2** and **4** are assigned to V and VI. The lowest energy band of the protonated species of **5** and **6** is located in a similar region to those of the protonated species V of **1–4**. Since the protonated species VII of **5** and **6** has a common π-electronic system to the protonated species V of **1–4**, it is reasonable to assign the protonated species of **5** and **6** to structure VII (Scheme 3).

As another protonated species of **1–4**, the generation of VIII was predicted by the Goto group.[13d] In the case of **1** and **2**, the generation of IX (R″ = H) is also possible by isomerizations of the protonated species V and VI. Similarly, the generation of IX would be postulated for the protonation of **5** and **6**. *O*-Ethyl derivative **5** and **6** cannot generate protonated species like VIII. On the other hand, we confirmed the spectroscopic similarity between the protonated species V of **1–4** and the protonated species VII of **5** and **6**. Thus, it is possible to exclude the generation of VIII for the protonation of **1–4**. The evidence that the
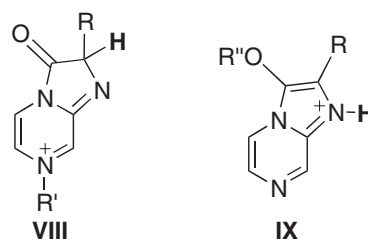
UV/vis absorption spectra of the protonated species of **1** and **2** were similar to those of the protonated species of the corresponding *N*-methyl derivatives **3** and **4**, respectively, excludes a possibility to generate IX, since *N*-methyl derivatives **3** and **4** cannot generate protonated species like IX. Therefore, we confirm the structures of the protonated species of **1–6**, as summarized in Scheme 3.

The data for the formation constants (Ks) for the protonations of **1–6** (Table 7) gave information about the thermodynamic parameters. Since methanesulfonic acid (**A–H**) was used for all protonation reactions of **1–6**, a difference in the K values originated from a free-energy difference (ΔG) between a neutral molecule (**IP**) and the corresponding protonated species (**IP + H**)$^+$ in Eq. 1. In the equilibrium of Eq. 1, an entropy change would be nearly constant for all protonation reactions of **1–6** in a specific solvent. Therefore, the K value reflects a difference of enthalpy ($\Delta\Delta H_f$) between **IP** and (**IP + H**)$^+$. In the protonated species of **1–6**, the protonated species V of *N*-methyl derivatives **3** and **4** have a common π-electronic system to the protonated species VII of the corresponding *O*-ethyl derivatives, **5** and **6**. Thus, the heat of formations (ΔH_f) of V for **3** and VII for **5** would be nearly the same as each other, and the heat of formations (ΔH_f) of V for **4** and VII for **6** are nearly the same as each other. Based on these evaluations, the energy diagrams for **3** and **5** and those for **4** and **6** are illustrated in Figs. 15 and 16, respectively. The ΔG values of *O*-ethyl derivatives **5** and **6** are much larger than those of the *N*-methyl derivatives, **3** and **4**, respectively. The enthalpy differences ($\Delta\Delta H_f$) between **3** and **5** were 5.6 and 8.2 kJ mol^{-1} in DMSO and methanol, respectively, and the $\Delta\Delta H_f$ values between **4** and **6** were 9.1 and 10.3 kJ mol^{-1} in DMSO and methanol, respectively. Thus, **3** and **4** are stabilized by a specific

S. Nakai et al.

Bull. Chem. Soc. Jpn., **76**, No. 12 (2003)   2373

in DMSO
for **3**   for **5**

in CH$_3$OH
for **3**   for **5**

Fig. 15. Energy diagram for protonations of **3** and **5** in DMSO and methanol at 25 °C.

in DMSO
for **4**   for **6**
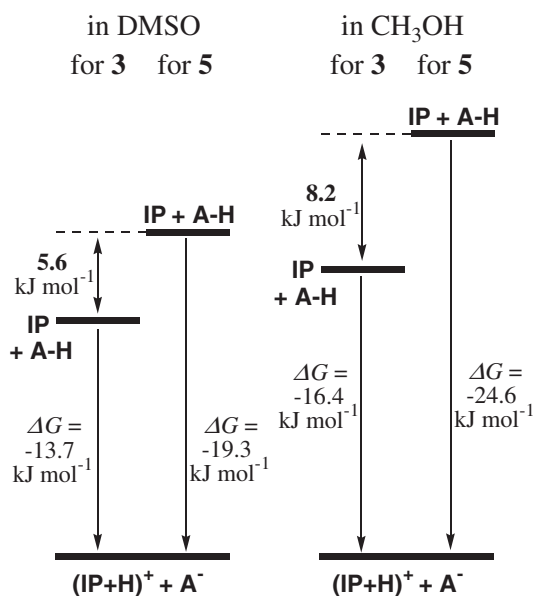
in CH$_3$OH
for **4**   for **6**

Fig. 16. Energy diagram for protonations of **4** and **6** in DMSO and methanol at 25 °C.

solvation interaction in DMSO and methanol more than **5** and **6**. One reason for this result is that a polarized character of **3** and **4** originated by the twitter ionic resonance structure **II** (Scheme 1) induces a strong interaction with solvent molecules. Especially, the $\Delta\Delta H_f$ value in methanol is larger than that in DMSO, indicating that the hydrogen bonding interaction with methanol molecules stabilizes **3** and **4** more than **5** and **6**. Furthermore, the $\Delta\Delta H_f$ values for the **4**/**6** system are larger than those for the **3**/**5** system, suggesting that the enlarged π-conjugated system containing the 2-phenyl group of **4** increases the stabilization effect by solvation, compared with 2-methyl derivative **3**. These results also match the conclusion that N–H derivatives **1** and **2** prefer to be the NH form isomer (**III**) in the tautomeric equilibrium (Scheme 2). The **III** form isomers of **1** and **2** may have a solvation interaction in a manner similar to those of **3** and **4**, and are stabilized more than the corresponding OH form isomers (**IV**).

(d) Effects of the Addition of a Base: In the presence of a base, an N–H imidazopyrazinone derivative, such as **1** and **2**, gives an anion species (deprotonated species), resulting in an UV/vis absorption spectral change.[13c,14] In this study, we reinvestigated the generation of anion species of **1** and **2** quantitatively by using 1,1,3,3-tetramethylguanidine (TMG) as a base. In the presence of TMG in DMSO and methanol, **1** and **2** showed spectral changes (Fig. 17), although alkylated derivatives **3**–**6** showed no spectral change. Since anion species of **1** and **2** were air-sensitive in an aprotic solvent owing to the chemiluminescent reactivity under air, their absorption spectra in DMSO were measured under N$_2$. In methanol, anion species of **1** and **2** had a moderate stability under air. Anion species of **1** showed absorption maxima at 450 and 405 nm in DMSO and methanol, respectively, and the anion species of **2** showed absorption maxima at 484 and 438 nm in DMSO and methanol, respectively. The data of anion species of **1** in methanol reproduced the reported values (400–405 nm) by Goto[13c] and Cormier.[14] The formation of anion species of **1** and **2** in meth-
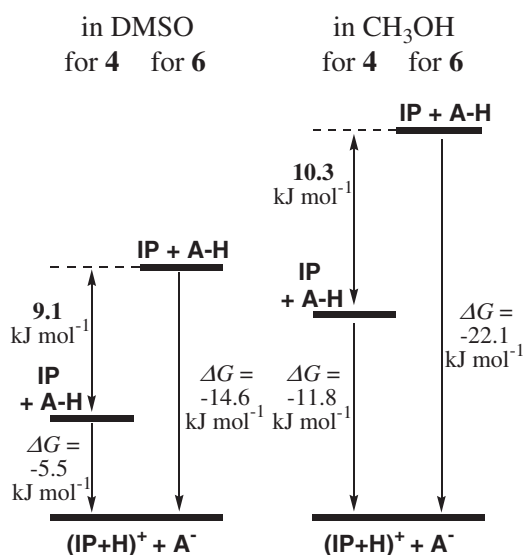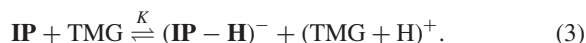
anol were followed by Eq. 3, where a neutral molecule (**IP**) and TMG give an anion species (**IP** − **H**)$^-$ and protonated TMG ((TMG + H)$^+$),

$$\mathbf{IP} + \mathrm{TMG} \overset{K}{\rightleftharpoons} (\mathbf{IP} - \mathbf{H})^- + (\mathrm{TMG} + \mathrm{H})^+. \quad (3)$$

The spectral changes of **1** and **2** were quantitatively analyzed using Eq. 4.[27] The value A_0 is the absorbance of **1** or **2** at a chosen wavelength in the absence of TMG. After the addition of TMG, an absorbance at the chosen wavelength is observed as A_{obs}. The difference between A_{obs} and A_0 is given by

$$A_{\mathrm{obs}} - A_0 = 0.5\Delta\varepsilon([\mathbf{IP}]_t + [\mathrm{TMG}]_t + 1/K - \{([\mathbf{IP}]_t \\ + [\mathrm{TMG}]_t + 1/K)^2 - 4[\mathbf{IP}]_t[\mathrm{TMG}]_t\}^{1/2}), \quad (4)$$

where $[\mathbf{IP}]_t$ and $[\mathrm{TMG}]_t$ are the initial concentrations of **1** or **2** and TMG, respectively, and $\Delta\varepsilon$ is the difference in the molar absorptivity between **1** or **2** and its anion species (**IP** − **H**)$^-$ at a chosen wavelength. The ($A_{\mathrm{obs}} - A_0$) values were plotted against the $[\mathrm{TMG}]_t$ values, as shown in Fig. 18, and the data were analyzed by a nonlinear least-squares curve fitting for Eq. 4. The K values for the deprotonation of **1** and **2** in methanol were obtained as 14800 ± 1300 and 100000 ± 21000, respectively. The $\Delta\varepsilon$ values at 422 nm for **1** and at 490 nm for **2** were estimated to be -2850 ± 90 and -7590 ± 250, respectively.

It is noteworthy that the anion species of **1** and **2** had a solvatochromic character. In addition to the data in DMSO and methanol, the lowest energy bands of the anion species of **1** were observed at 441, 416, and 395 nm in acetonitrile, 2-propanol, and water, respectively, and those of the anion species of **2** were observed at 475, 448, and 431 nm in acetonitrile, 2-propanol, methanol, and water, respectively. The wavenumbers (E_a (cm^{-1})) of the lowest energy bands of the anion species of **1** and **2** were correlated to the Kamlet–Taft's solvatochromic parameter α values,[26] accompanied by the data of the neutral form of **1** and **2** (Fig. 19). This spectroscopic observation indicates that anion species of **1** and **2** have an identical π-electronic character to the corresponding neutral molecules.
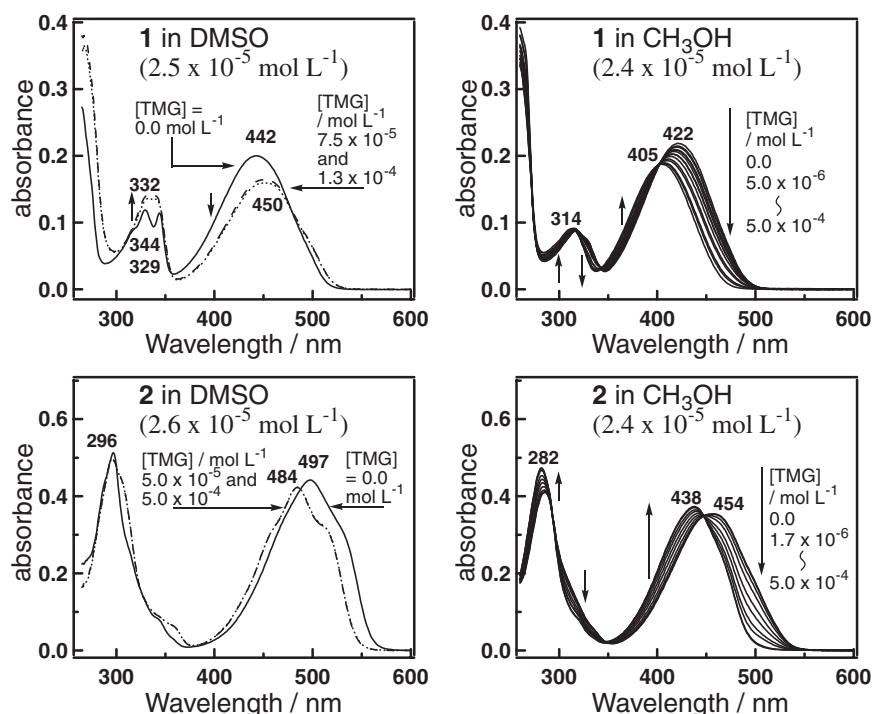
Fig. 17.   UV/vis absorption spectra of **1** and **2** in DMSO and methanol containing various concentrations of 1,1,3,3-tetramethyl-guanidine (TMG) at 25 ± 1 °C.
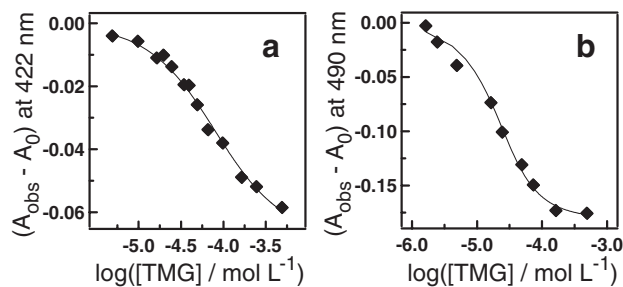

Fig. 18.   Plot of $(A_{obs} - A_0)$ at 422 nm vs [TMG] for deprotonation of **1** (**a**) and plot of $(A_{obs} - A_0)$ at 490 nm vs [TMG] for deprotonation of **2** (**b**) in methanol at 25 ± 1 °C. The solid lines correspond to the fitted curve to Eq. 4.

Fig. 19.   Plots of wavenumbers E_a (cm^{-1}) of the lowest energy bands for **1**, **2**, and the anion species $(\mathbf{IP} - \mathbf{H})^-$ of **1** and **2** against the Kamlet–Taft's α values.

These solvatochromic behaviors are caused by a hydrogen-bonding interaction where a hydrogen-bond donor part of solvent molecules interacts with a hydrogen-bond acceptor part of the anion species, and the energy levels of the frontier orbitals of the anion π-electronic systems are affected by hydrogen-bonding interactions.

When the solvatochromic property originated from a hydrogen-bonding interaction is used as a criterion for categorizing the imidazopyrazine π-electron system, the imidazopyrazinone derivatives **1**–**6** and their protonated species and anion species are classified into two categories, as shown in Scheme 4. Imidazopyrazinone derivatives **1**–**4**, the protonated species VI of **1**–**4**, and anion species $(\mathbf{IP} - \mathbf{H})^-$ of **1** and **2** are assigned into a 'solvatochromic group'. *O*-Ethyl derivatives **5** and **6**, the protonated species V of **1**–**4**, and the protonated species VII of **5** and **6** are assigned into a 'non-solvatochromic group'. It is obvious that two categories each have a common π-electronic structure. The compounds in the solvatochromic group have
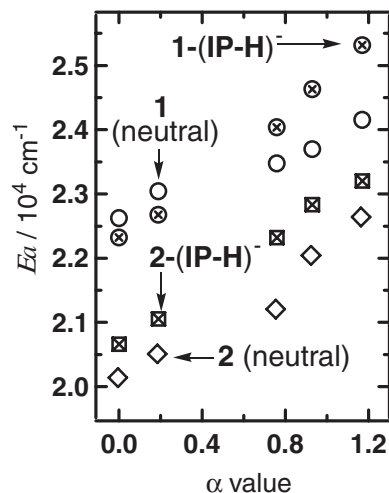
an imidazopyrazinone π-system which contains the conjugated p orbital of the oxygen atom O10. On the other hand, the compounds in the non-solvatochromic group have an imidazopyrazine π-system, which has only a conjugated interaction with the lone-pair electrons of the oxygen atom O10. Thus, the participation of the p orbital of the oxygen atom O10 into the imidazopyrazine π-system is important to determine the fundamental physical properties of the imidazopyrazinone derivatives.

5. NMR Spectra.   (a) ^{1}H NMR: In the pioneering work of the Goto group, ^{1}H NMR data of imidazopyrazinone derivatives **1**–**3** were well characterized.[13c,d] After their work, several groups reported different ^{1}H NMR data from those of the Goto
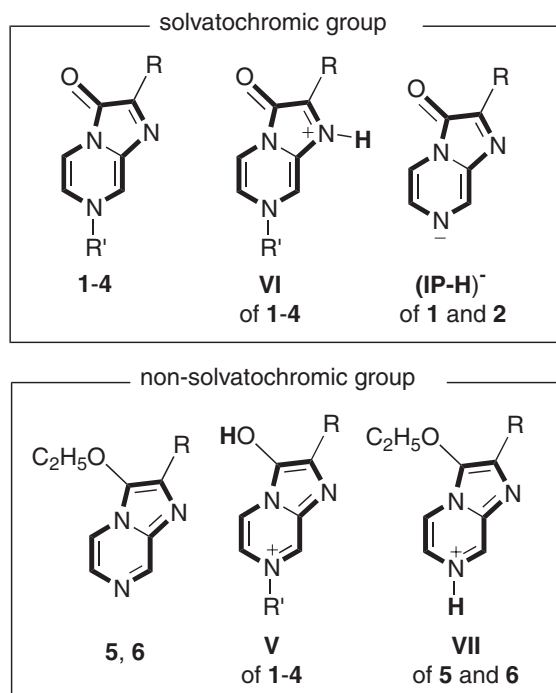
Scheme 4.

group, as summarized in Table 8, without any discussion.[12a,d,15] For instance, the Goto group reported the ^{1}H NMR data of two samples of **1** in DMSO-d_6; one was a neutral molecule of **1**, and the other was the HCl salt of **1**. The other groups showed ^{1}H NMR data of **1** similar to that of the HCl salt without any comments. To clarify the NMR spectroscopic characteristics of imidazopyrazinone derivatives, we systematically reinvestigated the ^{1}H NMR spectra of **1–6** as well as their ^{13}C NMR spectra.

^{1}H NMR data of **1–6** in DMSO-d_6 and CD$_3$OD are summarized in Table 9. Assignments of the protons were based on analyses of the results of ^{13}C NMR and 2D NMR (HMQC and HMBC) measurements. The ^{1}H NMR chemical shifts of **1–3** in DMSO-d_6 almost reproduced the reported data of the Goto group.[13c,d] The similarities of the ^{1}H shifts between **1** and **3** and the similarities of the ^{1}H shifts between **2** and **4** support that N–H derivatives **1** and **3** have preference of the NH form (**III**) over the OH form (**IV**) in tautomeric equilibrium in solutions, as concluded by using the results of UV/vis absorption measurements (Scheme 2). The ring protons, H$_{a-c}$, of *O*-ethyl derivatives **5** and **6** were more deshielded than those of **1–4**. This difference of the ^{1}H shifts was evaluated by comparing with reference compounds, pyrazine (**8**)[28] and a 1,4-dihydropyrazine derivative **9a**.[29] The ring protons of **8** and **9a** were reported to be 8.59 and 4.64 ppm (CDCl$_3$), respectively. The ^{1}H shifts of the ring protons of **1–4** are intermediate values between those of **8** and those of **9a**, suggesting that the imidazopyrazinone rings of **1–4** have small portions of aromatic (diatropic) character by a π-electronic resonance (Scheme 1). On the other hand, the ^{1}H shifts of the ring protons of **5** and **6** are close to those of **8**, suggesting that the π-electron ring systems of **5** and **6** have a moderate aromatic (diatropic) character.
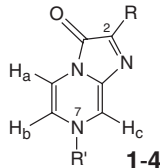
The ^{1}H NMR chemical shifts of **1–4** showed a characteristic dependency on a solvent, although those of **5** and **6** showed only a small solvent dependency. In the case of 2-methyl derivatives **1** and **3**, for instance, the ring protons H$_{a-c}$ were 0.15–0.30 ppm deshielded in CD$_3$OD more than the corresponding protons in DMSO-d_6. Especially, the ^{1}H shifts of H$_a$ of **1** and **3** showed a significant down-field shift ($\Delta\delta$ 0.30 and 0.27 ppm). 2-Methyl protons of **1** and **3** also showed deshielded ^{1}H shifts by a solvent change from DMSO-d_6 (2.28 and 2.27 ppm) to CD$_3$OD (2.43 and 2.42 ppm). In the case of 2-phenyl derivatives **2** and **4**, the ^{1}H shifts of H$_a$ and H$_b$ showed deshield-

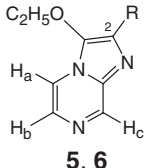Table 8. Reported ^{1}H NMR Data of Imidazopyrazinone Derivatives **1–3**

| Compound | Solvent | δ/ppm | | | | | Ref |
		H$_a$	H$_b$	N(7)H	H$_c$	Others	
1	DMSO-d_6	7.21	6.80	n.r.[b]	7.73	2.31 (2-Me)	13d
	DMSO-d_6 + HCl[a]	8.23	7.67	—	8.87	2.5 (2-Me)	13d
	DMSO-d_6 + HCl[a]	8.20	7.65	—	8.88	2.46 (2-Me)	12a
	MeOH-d_4 + HCl[a]	8.31	7.81	—	8.92	2.56 (2-Me)	12a
2	DMSO-d_6	7.3–7.6	6.89	3.30	8.04	7.3–7.6 (Ph, *p*- and *m*-), 8.41–8.64 (Ph, *o*-)	13c
	DMSO-d_6	6.81	7.28	n.r.[b]	7.88	n.r.[b]	15
	DMSO-d_6	7.63	7.04	n.r.[b]	8.25	7.33 (Ph, *p*-), 7.44 (Ph, *m*-), 8.43 (Ph, *o*-)	12a
	MeOH-d_4	8.29	7.70	n.r.[b]	8.86	n.r.[b]	12d
3	DMSO-d_6	7.22	6.70	—	7.71	2.28 (2-Me), 3.53 (7-Me)	13d

a) HCl salts of **1** were used for NMR measurements as the samples. b) Data was not reported.

Table 9. ^{1}H NMR Data of **1**–**6** in DMSO-d_6 and Methanol-d_4 at 25°C

Compound	Solvent	δ/ppm					J/Hz
		H_a	H_b	N(7)H	H_c	Others	
1	DMSO-d_6	7.16	6.77	10.6	7.70	2.28 (2-Me)	br[a)]
	MeOH-d_4	7.46	6.99	n.d.	7.85	2.43 (2-Me)	1.0 ($J_{b,c}$), 5.6 ($J_{a,b}$)
2	DMSO-d_6	7.4	6.90	11.3	8.06	7.34 (Ph, 4-), 7.45 (Ph, 3-), 8.49 (Ph, 2-)	br[a)]
	MeOH-d_4	7.61	7.03	n.d.	7.98	7.38 (Ph, 4-), 7.46 (Ph, 3-), 8.43 (Ph, 2-)	br[a)]
3	DMSO-d_6	7.21	6.70	—	7.71	2.27 (2-Me), 3.52 (7-Me)	1.6 ($J_{b,c}$), 5.9 ($J_{a,b}$)
	MeOH-d_4	7.48	6.93	—	7.86	2.42 (2-Me), 3.72 (7-Me)	1.3 ($J_{b,c}$), 5.9 ($J_{a,b}$)
4	DMSO-d_6	7.50	6.85	—	8.08	3.64 (7-Me), 7.33 (Ph, 4-), 7.45 (Ph, 3-), 8.47 (Ph, 2-)	1.3 ($J_{b,c}$), 5.6 ($J_{a,b}$)
	MeOH-d_4	7.62	6.96	—	7.98	3.78 (7-Me), 7.37 (Ph, 4-), 7.46 (Ph, 3-), 8.43 (Ph, 2-)	1.3 ($J_{b,c}$), 5.6 ($J_{a,b}$)
5	DMSO-d_6	8.23	7.80	—	8.81	1.35 (OEt), 2.37 (2-Me), 4.23 (OEt)	1.3 ($J_{a,c}$), 4.6 ($J_{a,b}$), 7.1 (OEt)
	MeOH-d_4	8.18	7.82	—	8.75	1.44 (OEt), 2.46 (2-Me), 4.30 (OEt)	1.6 ($J_{a,c}$), 4.6 ($J_{a,b}$), 7.1 (OEt)
6	DMSO-d_6	8.39	7.89	—	8.99	1.42 (OEt), 4.24 (OEt), 7.38 (Ph, 4-), 7.52 (Ph, 3-), 8.09 (Ph, 2-)	1.3 ($J_{a,c}$), 4.6 ($J_{a,b}$), 6.9 (OEt)
	MeOH-d_4	8.29	7.87	—	8.88	1.44 (OEt), 4.24 (OEt), 7.39 (Ph, 4-), 7.50 (Ph, 3-), 8.05 (Ph, 2-)	1.3 ($J_{a,c}$), 4.6 ($J_{a,b}$), 7.1 (OEt)

a) Broad peaks were observed.

ed values in CD$_3$OD compared with those in DMSO-d_6, although the ^{1}H shifts of H_c showed slightly shielded values in CD$_3$OD relative to those in DMSO-d_6. These results suggest that a diatoropic character of the imidazopyrazinone rings of **1**–**4** is slightly increased in a protic solvent, such as CD$_3$OD, more than in an aprotic solvent, such as DMSO-d_6. The ^{1}H shifts of 2-methyl groups of **1** and **3** may also be affected by an increased diamagnetic ring current in CD$_3$OD. The ring protons, H_{a-c}, of 2-phenyl derivatives **2** and **4** were shifted to a downfield region relative to those of the corresponding 2-methyl derivatives, **1** and **3**. This result would be caused by a diamagnetic ring current of their phenyl groups and/or by a conjugation effect. A similar downfield shift by phenyl-substitution was also observed in *O*-ethyl derivatives **6** relative to **5**. In the phenyl protons of **2**, **4**, and **6**, the *ortho* protons showed characteristic chemical shifts. The *ortho* protons of **2** and **4** (8.43–8.49 ppm) were more deshielded than those of **6** (8.05–8.09 ppm). One of the explanations for this difference is that the *ortho* protons of **2** and **4** are deshielded by a diamagnetic anisotropy effect from the carbonyl C3–O10 bonds, while there is no such effect for **6**.

A characteristic difference between **1**–**4** and **5**–**6** also appeared in the coupling constants (*J*). The $J_{a,b}$ values of **1**–**4** (5.6–5.9 Hz) were larger than those of **5** and **6** (4.6 Hz). In the case of **1**–**4**, small $J_{b,c}$ values were observed (1.0–1.6 Hz). On the other hand, **5** and **6** showed small $J_{a,c}$ values (1.3–1.6

Hz), while the $J_{b,c}$ values were nearly 0 Hz. The *J* values of **1**–**3** reproduce the values reported by the Goto group.[13c,d] The $J_{2,3}$ values of pyrazine derivatives[28] and 1,4-dihydropyrazine derivatives[30] were 2.5–3 Hz and 6.4–6.5 Hz, respectively. Thus, the pyrazine parts of **1**–**4** have a similar structural characteristic to the 1,4-dihydropyrazine derivatives compared with the pyrazine parts of **5** and **6**.

(b) ^{13}C NMR: ^{13}C NMR data of **1**–**6** in DMSO-d_6 and CD$_3$OD are listed in Table 10. These data are slightly different from the reported values.[12a] The chemical shifts of the ring carbons for **1**–**6** were slightly deshielded in CD$_3$OD compared with those in DMSO-d_6 ($\Delta\delta$ 0.0–3.7 ppm). In the case of **1**–**4**, C3 showed the most deshielded chemical shifts in the carbons of the imidazopyrazinone rings. The ^{13}C shifts of C3 for **1**–**4** (152–154 ppm) were far upfield compared with those of the carbonyl carbons of unsaturated cyclic ketones, such as tropone **7** (187.7 ppm) and *p*-benzoquinone (187.0 ppm).[31] This evaluation strongly supports that the imidazopyrazinone rings of **1**–**4** have a character of the zwitter-ionic resonance structure **II** and possess the weakened carbonyl character of C3–O10 bonds (Scheme 1). In the case of **5** and **6**, the chemicals shifts of C8 had the most deshielded values (142–144 ppm) in the imidazopyrazinone ring carbons. In the partial pyrazine ring, the ^{13}C shifts of the C5–C6 and C8–C9 parts of **1**–**4** were observed at 109–121 and 121–131 ppm, respectively, and the ^{13}C shifts of the C5–C6 and C8–C9 parts of **5** and **6** were

Table 10. ^{13}C NMR Data of **1**–**6** in DMSO-d_6 and Methanol-d_4 at 25 °C

Compound	Solvent	δ/ppm						
		C2	C3	C5	C6	C8	C9	Others
1	DMSO-d_6	147.3[a]	152.4[a]	109.1[a]	115.1[a]	120.7[a]	128.9[a]	13.68 (2-Me)
	MeOH-d_4	147.5[a]	153.4[a]	111.64	117.4[a]	124.4[a]	130.3[a]	13.65 (2-Me)
2	DMSO-d_6	140.5[a]	151.6[a]	111.52	114.8[a]	124.2[a]	129.0[a]	133.76 (Ph, 1-), 125.99 (Ph, 2-), 128.33 (Ph, 3-), (128.13 (Ph, 4-)
	MeOH-d_4	143.0[b]	153.03	113.12	117.04	126.18	130.83	134.40 (Ph, 1-), 128.07 (Ph, 2-), 129.61 (Ph, 3-), 130.15 (Ph, 4-)
3	DMSO-d_6	147.02	152.37	109.42	119.30	124.25	128.85	13.73 (2-Me), 41.96 (7-Me)
	MeOH-d_4	147.64	153.59	111.86	121.46	127.84	130.49	13.68 (2-Me), 43.79 (7-Me)
4	DMSO-d_6	140.17	151.70	111.87	118.95	127.56	129.05	42.73 (7-Me), 133.78 (Ph, 1-), 125.92 (Ph, 2-), 128.31 (Ph, 3-), 128.08 (Ph, 4-)
	MeOH-d_4	143.27	153.18	113.36	121.06	129.45	131.07	44.19 (7-Me), 134.52 (Ph, 1-), 128.05 (Ph, 2-), 129.60 (Ph, 3-), 130.12 (Ph, 4-)
5	DMSO-d_6	129.99	135.75	115.05	128.40	141.79	132.86	12.38 (2-Me), 15.20 (OEt), 70.53 (OEt)
	MeOH-d_4	131.97	138.26	116.64	129.67	142.53	134.68	12.49 (2-Me), 15.86 (OEt), 72.35 (OEt)
6	DMSO-d_6	130.57	135.72	115.68	128.77	142.93	133.52	15.18 (OEt), 70.52 (OEt), 132.40 (Ph, 1-), 126.02 (Ph, 2-), 128.77 (Ph, 3-), 127.96 (Ph, 4-)
	MeOH-d_4	133.50	137.96	117.06	129.95	143.59	135.44	15.77 (OEt), 72.19 (OEt), 133.45 (Ph, 1-), 128.05 (Ph, 2-), 129.97 (Ph, 3-), 129.69 (Ph, 4-)

a) Broad peaks were observed.

observed at 115–130 and 133–144 ppm, respectively. The ring carbons of **1**–**4** were shielded compared with those of **5** and **6**, supporting the idea that the aromatic (diatropic) character of the imidazopyrazinone rings of **1**–**4** is smaller than that of **5** and **6**. It is one of the characteristics of the fused ring structure for **1**–**6** that the carbons of the C8–C9 parts were deshielded more than those of the C5–C6 parts. As another characteristic, the ^{13}C shifts of the carbons of the pyrazine parts of **1**–**6** were almost observed within the range between the ^{13}C shifts of the ring carbons of 1,4-dihydropyrazine derivative **9b** (116 ppm)[32] and pyrazine **8** (145 ppm).[31]

(c) **Protonated Species and Anion Species:** In the presence of methanesulfonic acid (MSA) in DMSO-d_6 and CD$_3$OD, ^{1}H NMR spectra of **1**–**6** showed the characteristic ^{1}H shifts of the protonated species (Table 11). For **1**, the ^{1}H NMR spectra of the protonated species didn't match the reported data of the HCl salts of **1**,[12a,13d] suggesting that the data for the HCl salts of **1** reflected a tendency of a protonation equilibrium. Protonated species of **1**–**4** showed H$_a$, H$_b$, and H$_c$ at 8.3–8.5, 7.7–7.9, and 9.0–9.3 ppm, respectively, and protonated species of **5** and **6** showed H$_a$, H$_b$, and H$_c$ at 8.6–8.9, 8.1–8.2, and 9.2–9.6 ppm, respectively. Thus, the ring protons of the protonated species

of **5** and **6** were slightly deshielded compared with those of the protonated species of **1**–**4**. An origin of this difference would be the difference in the contributed isomers of the protonated species, as shown in Scheme 3. The data of the protonated species of **1**–**4** would contain the spectral characteristics of structures V and VI, and those of the protonated species of **5** and **6** would contain the spectral characteristics of VII mainly. The 2-methyl protons of the protonated species of **5** and the *ortho* protons on the 2-phenyl group of the protonated species of **6** were more deshielded than those of the corresponding neutral molecules. This downfield shift would be caused by an electron deficient property of the imidazopyrazine ring in the protonated structure VII of **5** and **6**. Similarly, the 2-methyl protons of the protonated species of **1** and **3** were more deshielded than those of the corresponding neutral molecules. On the other hand, the *ortho* protons on the 2-phenyl groups of the protonated species of **2** and **4** were more shielded than those of the neutral molecules. One of the reasons for these upfield shifts of the *ortho* protons is that a diamagnetic anisotropy effect from the carbonyl C3–O10 bonds of the neutral molecules of **2** and **4** is diminished by protonations on O10, which give protonated species V.

Table 11. ^{1}H NMR Data of **1–6** (0.030 mol L^{-1}) in DMSO-d_6 and Methanol-d_4 in the Presence of MSA[a] at 25 °C

| Compound	Solvent	δ/ppm				J/Hz
		H$_a$	H$_b$	H$_c$	Others	
1	DMSO-d_6	8.38	7.92	9.17	2.53 (2-Me)	5.6 ($J_{a,b}$)
	MeOH-d_4	8.37	7.93	9.07	2.60 (2-Me)	1.0 ($J_{a,c}$), 5.3 ($J_{a,b}$)
2	DMSO-d_6	8.47	7.85	9.22	7.49 (Ph, 4-), 7.59 (Ph, 3-), 8.28 (Ph, 2-)	5.6 ($J_{a,b}$)
	MeOH-d_4	8.43	7.85	9.07	7.51 (Ph, 4-), 7.57 (Ph, 3-), 8.25 (Ph, 2-)	1.0 ($J_{a,c}$), 0.7 ($J_{b,c}$), 5.6 ($J_{a,b}$)
3	DMSO-d_6	8.39	7.84	9.23	2.53 (2-Me), 4.11 (7-Me)	1.3 ($J_{b,c}$), 5.6 ($J_{a,b}$)
	MeOH-d_4	8.34	7.81	9.09	2.59 (2-Me), 4.18 (7-Me)	1.3 ($J_{b,c}$), 5.6 ($J_{a,b}$), 5.9 ($J_{a,b}$)
4	DMSO-d_6	8.48	7.83	9.25	4.12 (7-Me), 7.48 (Ph, 4-), 7.57 (Ph, 3-), 8.27 (Ph, 2-)	
	MeOH-d_4	8.39	7.76	9.06	4.18 (7-Me), 7.49 (Ph, 4-), 7.55 (Ph, 3-), 8.24 (Ph, 2-)	1.3 ($J_{b,c}$), 5.9 ($J_{a,b}$)
5	DMSO-d_6	8.72	8.20	9.24	1.43 (OEt), 2.58 (2-Me), 4.46 (OEt)	4.9 ($J_{a,b}$), 7.1 (OEt)
	MeOH-d_4	8.61	8.18	9.25	1.53 (OEt), 2.65 (2-Me), 4.53 (OEt)	1.0 ($J_{a,c}$), 4.9 ($J_{a,b}$), 6.9 (OEt)
6	DMSO-d_6	8.93	8.17	9.62	1.46 (OEt), 4.40 (OEt), 7.55 (Ph, 4-), 7.63 (Ph, 3-), 8.16 (Ph, 2-)	1.0 ($J_{a,c}$), 5.3 ($J_{a,b}$), 7.1 (OEt)
	MeOH-d_4	8.78	8.11	9.36	1.51 (OEt), 4.42 (OEt), 7.53 (Ph, 4-), 7.59 (Ph, 3-), 8.14 (Ph, 2-)	1.0 ($J_{a,c}$), 0.7 ($J_{b,c}$), 5.3 ($J_{a,b}$), 6.9 (OEt)

a) Concentrations of MSA (methanesulfonic acid) were 2.0 and 0.2 mol L^{-1} in DMSO and MeOH, respectively.

Table 12. ^{1}H NMR Data of **1** and **2** in DMSO-d_6 and Methanol-d_4 in the Presence of TMG (0.10 mol L^{-1}) at 25 °C

Compound	Solvent	δ/ppm				J/Hz
		H$_a$	H$_b$	H$_c$	Others	
1	DMSO-d_6	7.03	7.35	7.92	2.14 (2-Me)	1.0 ($J_{b,c}$), 4.6 ($J_{a,b}$)
	MeOH-d_4	7.35	7.78	8.22	2.35 (2-Me)	1.3 ($J_{b,c}$), 4.6 ($J_{a,b}$)
2	DMSO-d_6	7.09	7.51	8.14	6.94 (Ph, 4-), 7.23 (Ph, 3-), 8.30 (Ph, 2-)	1.3 ($J_{b,c}$), 4.6 ($J_{a,b}$)
	MeOH-d_4	7.38	7.87	8.37	7.15 (Ph, 4-), 7.36 (Ph, 3-), 8.29 (Ph, 2-)	1.3 ($J_{b,c}$), 4.9 ($J_{a,b}$)

In the presence of 1,1,3,3-tetramethylguanidine (TMG) in DMSO-d_6 and CD$_3$OD, **1** and **2** showed ^{1}H NMR spectral changes caused by the generation of anion species $(\mathbf{IP-H})^-$ (Table 12), although **3–6** showed no spectral change. The 2-methyl protons of the anion species of **1** and the *ortho* protons on the 2-phenyl group of the anion species of **2** showed shielded chemical shifts compared with those of the corresponding neutral molecules. Thus, the imidazopyrazinone ring of $(\mathbf{IP-H})^-$ has an electron-donating property for both inductive and resonance effects compared with that of the neutral molecule. As another characteristic, protons H$_b$ and H$_c$ of the anion species of **1** and **2** showed deshielded chemical shifts compared with those of the corresponding neutral molecules, while their protons, H$_a$, showed small upfield shifts. This downfield shift of protons H$_b$ and H$_c$ of the anion species would have originated from a diatropic character of the resonance structure. Anion species $(\mathbf{IP-H})^-$ may be contributed by the resonance structures X and XI (Scheme 5), and the NMR property of $(\mathbf{IP-H})^-$ reflects a diatropic character of the resonance structure XI,
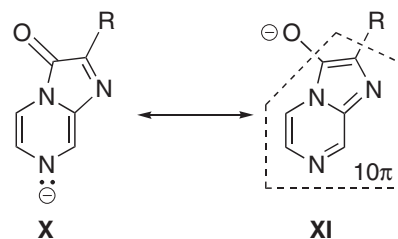
Scheme 5.

which has a 10π electron ring system with a localized negative charge on O10. In addition, the coupling constants $J_{a,b}$ (4.6 Hz) of $(\mathbf{IP-H})^-$ were similar to those of **5** and **6**, which possess the 10π electron imidazopyrazine rings, to support a contribution of the resonance structure XI into the π-electronic system of the anion species $(\mathbf{IP-H})^-$.

6. Molecular Orbital Considerations. (a) Structures of Imidazopyrazinone Derivatives: To evaluate the structural

Table 13. Calculated Properties of Imidazopyrazinone Derivatives **1–4** in Gas Phase and in DMSO with the AM1-COSMO Method

| Compound | In gas phase ($\varepsilon = 1.0$) | | | | |
	ΔH_f[a)]/kJ mol^{-1}	Angle[b)]	C3–O10 bond length/Å	Net atomic charge on O(10)	μ[c)]/D
1	227.2	150.4°	1.235	−0.32	3.7
2	368.5	153.0°	1.236	−0.33	3.8
3	246.6	155.8°	1.235	−0.32	4.2
4	387.9	158.6°	1.236	−0.33	4.3
Compound	In DMSO ($\varepsilon = 46.5$)				
	ΔH_f[a)]/kJ mol^{-1}	Angle[b)]	C3–O10 bond length/Å	Net atomic charge on O(10)	μ[c)]/D
1	133.0	177.2°	1.262	−0.57	13.2
2	267.5	176.9°	1.260	−0.55	15.3
3	164.6	176.6°	1.260	−0.56	12.5
4	300.2	176.3°	1.259	−0.54	14.6

a) Heat of formation. b) Angle N(4)–N(7)–H(11) or angle N(4)–N(7)–C(11). c) Dipole moment.

characteristics of imidazopyrazinone derivatives observed by X-ray crystallographic analyses, AM1 semi-empirical MO calculations of imidazopyrazinone derivatives were carried out (Table 13).[33] The optimized geometries of **1–4** in the gas phase ($\varepsilon = 1.0$) had a bending imidazopyrazinone ring, in which the hydrogen atoms or the methyl groups at N7 exist out of the plane made by the imidazopyrazinone ring. The angles N4–N7–H11 of **1** and **2** were ca. 150°, and the angles N4–N7–C11 of **3** and **4** were ca. 160°. These bent structures are different from the observed crystal structures of **2–4**. Thus, we also optimized the geometries of **1–4** using the AM1-COSMO solvation model.[34] AM1-COSMO calculations for a representative compound **1** were carried out with various dielectric constant values ($\varepsilon = 2.5, 5.0, 10.0, 20.0, 40.0,$ and 78.3) as shown in Fig. 20. The optimized heat of formation (ΔH_f) rapidly decreased with an increase of the ε value, and the angle N4–N7–H11 reached 177° at $\varepsilon = 5.0$. The planar structure of the imidazopyrazinone ring is preferable under the conditions where the ε value is larger than 5.0. A rapid increase of the dipole moment (μ) with an increase of the ε value also synchronized with a rapid decrease of the ΔH_f value (Fig. 20c). The calculation results for **1–4** using the AM1-COSMO method ($\varepsilon = 46.5$) are summarized in Table 13. The optimized planar imidazopyrazinone ring structures could reproduce the planar structures of **2–4** observed by X-ray crystallography. The calculated C3–O10 bond lengths of **1–4** reproduced the characteristic lengths (1.25–1.26 Å) for **2–4** observed by X-ray crystallography, and the net atomic charges on O10 were calculated as ca. −0.6. This result supports that an imidazopyrazinone derivative is contributed by the zwitter-ionic resonance structure **II**, and has a weakened carbonyl C3–O10 bond (Scheme 1). The calculated dipole moments (μ) for **1–4** were 12–15 D. These values are larger than those of tropone **7** (4.3 D)[35,36] and 4-nitrodimethylaniline **10** (7.1 D),[37] and are comparable to that of pyridinium cyclopentadienide **11** (13 D).[25,38]

(b) **Tautomeric Isomerization:** The results of spectral measurements for **1–6** indicate that N–H derivatives **1** and **2** prefer to be the NH forms (**III**) over the OH forms (**IV**) in the tautomeric equilibriums (Scheme 2). To support this conclusion, the differences of the heats of formation (ΔH_f) between the **III**
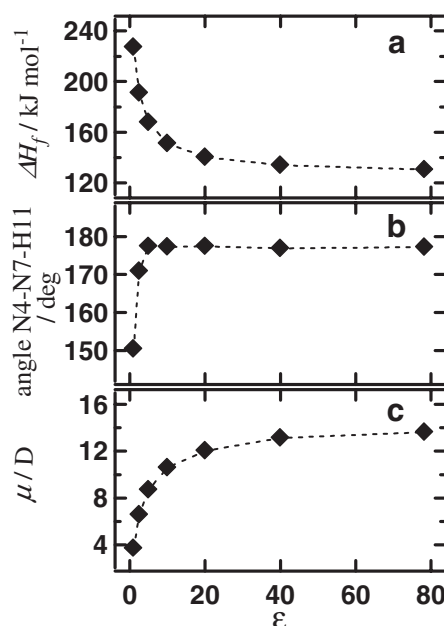

Fig. 20. Plots of (**a**) heat of formation ((ΔH_f), (**b**) angle N(4)–N(7)–H(11), and (**c**) dipole moment (μ) of **1** calculated with the AM1-COSMO method against dielectric constants ε.
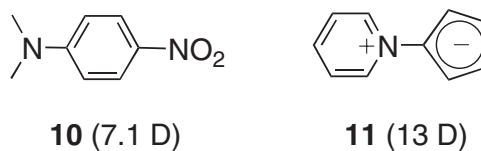

10 (7.1 D) **11** (13 D)

Chart 4.

form and the **IV** form for **1** and **2** were evaluated by using the AM1-COSMO method with various dielectric constant values ($\varepsilon = 1.0, 2.5, 5.0, 10.0, 20.0, 40.0,$ and 78.3). The optimized ΔH_f values were plotted against the ε value, as shown in Fig. 21. In the gas phase ($\varepsilon = 1.0$), the ΔH_f values of the **IV** forms were smaller than those of the **III** forms. When the ε val-
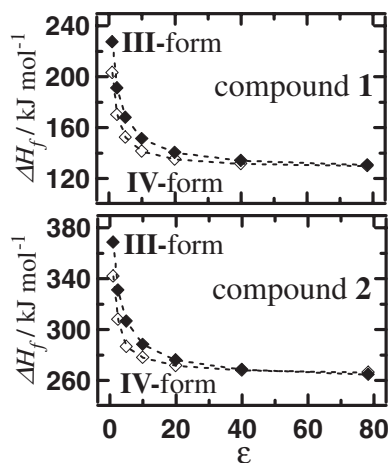
Fig. 21. Heat of formation (ΔH_f) of the III and IV forms for **1** and **2** calculated with the AM1-COSMO method plotted against dielectric constants ε.

ue increases, the ΔH_f value of the III form decreased more rapidly than that of the IV form. The $\Delta\Delta H_f$ values in water ($\varepsilon = 78.3$) for **1** and **2** were estimated to be 0.8 and -1.5 kJ mol^{-1}, respectively. These calculation results are in conflict with the conclusion about the tautomeric equilibrium of **1** and **2**. The evaluation of the K values for the protonations of **1**–**6** confirms that imidazopyrazinone derivatives **1**–**4** are stabilized by a specific solvation interaction in solutions more than **5** and **6**. Thus, AM1-MO calculations could not reproduce the experimental observations concerning the heats of formation, as shown in Figs. 15 and 16, since the specific solvation effect for imidazopyrazinone derivatives is not considered in this solvation model.[34]

(c) Spectroscopic Character of 1–6: The evidence that the spectroscopic properties of **1**–**4** were different from those of **5** and **6** was supported by the AM1-MO calculations. Before evaluating the calculation results, the dependency of the MO energy levels of **1** and **2** (the III forms) upon the ε values was studied by the AM1-COSMO method ($\varepsilon = 1.0$, 2.5, 5.0, 10.0, 20.0, 40.0, and 78.3), as shown in Fig. 22. The energy levels of HOMO and LUMO showed characteristic changes dependent upon the ε values in a manner similar to the ΔH_f values (Fig. 20). Since the energy levels of HOMO and LUMO showed only small change in the range of the ε values (19.9–78.3) of the solvents employed for the spectroscopic measurements in this research, the solvatochromic character of **1**–**4** cannot be explained only by the effect of the dielectric character of the medium in the MO calculations.

The MO characters of **1**–**6** were evaluated using the results of the AM1-COSMO calculations ($\varepsilon = 46.5$). Figure 23 illustrates the energy levels of HOMO, LUMO, HOMO+1, and LUMO+1 of **1**–**4** accompanied by those of **5′** and **6′**. To evaluate the property of *O*-ethyl derivatives **5** and **6**, AM1-COSMO calculations of *O*-methyl derivatives **5′** and **6′** were carried out as simpler structure models. The results that the HOMO–LUMO energy gaps of **1**–**4** (6.6–7.0 eV) are much smaller than those of **5′** and **6′** (8.2–8.5 eV) match the observation that the lowest energy bands of **1**–**4** appeared in the low-energy region compared with those of **5** and **6**. The difference in the HOMO–LUMO energy gaps between **1**–**4** and **5′**–**6′** mainly results from
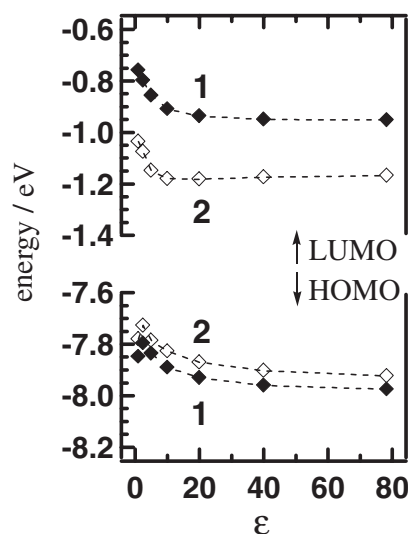

Fig. 22. Energy levels of HOMO and LUMO of **1** and **2** calculated with the AM1-COSMO method plotted against dielectric constants ε.

the difference in the energy levels of the HOMOs. The energy levels of the HOMOs (> -8.0 eV) of **1**–**4** are ca. 1.5 eV higher than those (< -9.0 eV) of **5′** and **6′**. The energy levels of HOMOs and LUMOs of **5′** and **6′** are similar to those of HOMO (-9.03 eV) and LUMO (-0.59 eV) of naphthalene, a typical 10π aromatic compound, calculated by the AM1-COMSO ($\varepsilon = 46.5$). Thus, it is a notable characteristic of the imidazopyrazinone π-electronic structure that the energy levels of the HOMOs of **1**–**4** are higher than those of **5′** and **6′**.

The calculation data for the HOMO–LUMO energy levels (Fig. 23) also support the methyl- and phenyl-substituent effects on the spectroscopic property in **1**–**4**. The HOMO–LUMO energy gaps of *N*-methyl derivatives **3** and **4** are smaller than those of the corresponding N–H derivatives **1** and **2**, respectively. This result matches the observation that the lowest energy bands of **3** and **4** showed a red-shift comparable with those of **1** and **2**. The red-shifted lowest energy bands of 2-phenyl derivatives **2** and **4** compared with those of 2-methyl derivatives **1** and **3** are also supported by calculation results that the HOMO–LUMO energy gaps for **2** and **4** are smaller than those of **1** and **3**.

(d) Solvatochromism: As another notable spectroscopic character, **1**–**4** showed solvatochromism originating from hydrogen-bonding interactions with solvent molecules. As noted above, the results of the AM1-COSMO calculations for **1**–**4** with various ε values could not explain the solvatochromism. To understand the origin of the solvatochromism, we need to evaluate a specific effect of the hydrogen-bonding interaction on the energy levels of the frontier orbitals of an imidazopyrazinone derivative. In hydrogen bonding interactions, a hydrogen-bond acceptor part of an imidazopyrazinone derivative interacts with a hydrogen-bond donor part of solvent molecules. The imidazopyrazinone π-system has a character of the zwitter-ionic resonance structure II possessing a localized negative charge on O10. The AM1-COSMO calculations of **1**–**4** also indicated that the imidazopyrazinone structure has a large negative charge localized on O10 (Table 13), suggesting that the
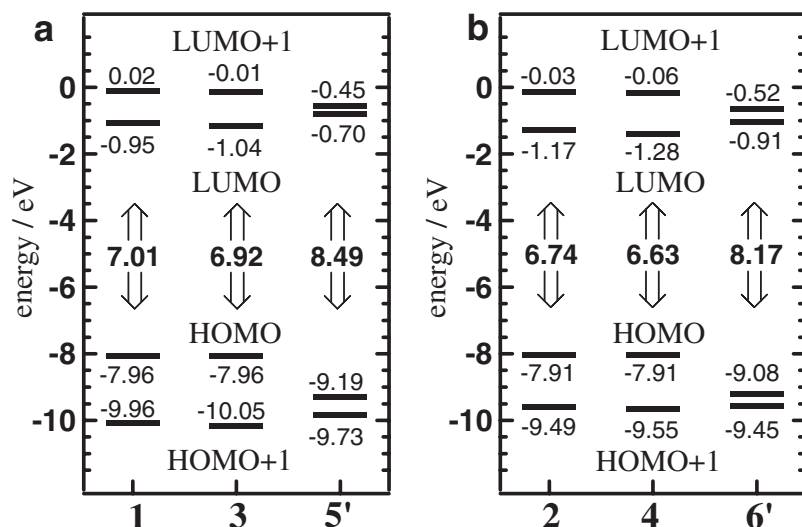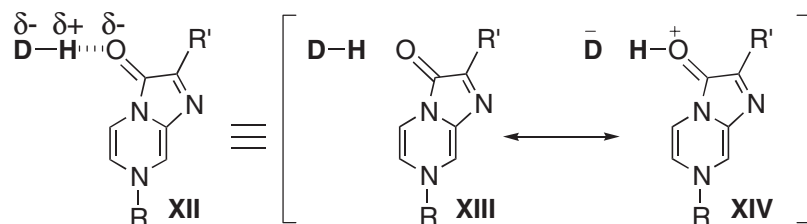
S. Nakai et al.

Bull. Chem. Soc. Jpn., **76**, No. 12 (2003) 2381

Fig. 23.   Energy levels of HOMO, LUMO, HOMO+1, and LUMO+1 for **1**, **3**, and **5′** (**a**) and for **2**, **4**, and **6′** (**b**) calculated with the AM1-COSMO method ($\varepsilon = 46.5$). The HOMO–LUMO energy gaps are shown with arrows.

Scheme 6.

oxygen atom O10 works as the hydrogen-bond acceptor part. Thus, we describe a hydrogen-bonded structure XII of an imidazopyrazinone derivative with a hydrogen-bond donor molecule (**D–H**) by resonance structures XIII and XIV, as shown in Scheme 6.[39,40] The resonance structure XIII contains an imidazopyrazinone part, whose electronic property is identical to that of the free imidazopyrazinone molecule, and XIV contains an imidazopyrazinone part whose electronic property is identical to that of the protonated species V. By using a valence-bond method, the wave function of XII (Ψ(XII)) is represented by Eq. 5, where Ψ(XIII) and Ψ(XIV) denote the wave functions for XIII and XIV, respectively:

$$\Psi(\text{XII}) = a\Psi(\text{XIII}) + b\Psi(\text{XIV}). \tag{5}$$

In the case of **1**, for instance, the neutral molecule and the protonated species V showed the lowest energy band at 442 and 382 nm in DMSO ($\alpha = 0$). The neutral molecule of **1** in water ($\alpha = 1.17$) showed the lowest energy band at an intermediate wavelength (414 nm). Thus, the hydrogen-bonded structure XII for **1** in water has contributions of both Ψ(XIII) and Ψ(XIV) in a similar extent to each other ($a \cong b$). In a solvent whose Kamlet–Taft's α value is smaller than that of water ($1.2 > \alpha > 0$), the contribution of Ψ(XIII) increases over that of Ψ(XIV) in the hydrogen-bonded structure XII ($a > b$). Then, the ratio a/b in this solvent becomes larger than that in water and the lowest energy band is shifted to the red region compared with that in water.

(e) Protonated Species and Anion Species: Basis on the

assignment by the Goto group,[13d] the protonated species of **1–4** were assigned to V and VI, and the protonated species of **5** and **6** were assigned to VII (Scheme 3). To understand the properties of these ptotonated species, AM1-COSMO calculations ($\varepsilon = 46.5$) of the protonated species V and VI of **1–4** were carried out (Table 14). Table 15 summarizes the calculated properties of the protonated species VII of **5′** and **6′** accompanied by those of neutral molecules **5′** and **6′**. Experimentally, the protonated species V of **1–4** have blue-shifted lowest energy bands compared with those of the corresponding neutral molecules, and the protonated species VI have red-shifted lowest energy bands. The calculated HOMO–LUMO energy gaps are consistent with the observed spectroscopic character of V and VI for **1–4**. The HOMO–LUMO energy gap of V for **1** (8.04 eV), for instance, is larger than that of the neutral molecule (7.01 eV) and the HOMO–LUMO energy gap of VI for **1** (6.79 eV) is smaller than that of the neutral molecule.
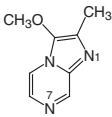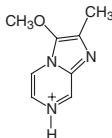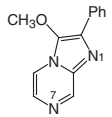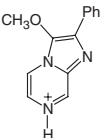
The protonated species VII of **5** and **6** showed the red-shifted lowest energy bands compared with the corresponding neutral molecules. While the protonated species VII of **5** and **6** have common π-electronic systems to the protonated species V of **1–4**, the observed lowest energy bands of VII for **5** and **6** showed blue shifts compared with those of the corresponding protonated species V for **1** (or **3**) and **2** (or **4**), respectively. MO calculations showed that the HOMO–LUMO energy gaps of VII for **5′** and **6′** were smaller than those of the corresponding neutral molecules, and were larger than those of the corresponding protonated species V for **1** (or **3**) and **2** (or **4**), respectively. Thus,

Table 14.   Properties of the Protonated Species V and VI of **1**–**4** Calculated with the AM1-COSMO Method ($\varepsilon = 46.5$)

	V(**1**)	VI(**1**)	V(**2**)	VI(**2**)	V(**3**)	VI(**3**)	V(**4**)	VI(**4**)
$\Delta H_f{}^{a)}$/kJ mol^{-1}	569.0	563.9	706.1	700.8	606.4	599.7	743.6	737.7
HOMO (eV)	−9.48	−8.41	−9.27	−8.30	−9.47	−8.40	−9.25	−8.31
LUMO (eV)	−1.44	−1.62	−1.49	−1.81	−1.60	−1.75	−1.64	−1.95
ΔE(HOMO–LUMO)$^{b)}$/eV	8.04	6.79	7.78	6.49	7.87	6.66	7.61	6.36
Net atomic charge on O(10)	−0.27	−0.55	−0.27	−0.52	−0.27	−0.54	−0.26	−0.51

a) Heat of formation. b) HOMO–LUMO energy gap.

Table 15.   Properties of **5′**, **6′**, and Their Protonated Species VII Calculated with the AM1-COSMO Method ($\varepsilon = 46.5$)

	5′	VII(**5′**)	**6′**	VII(**6′**)
$\Delta H_f{}^{a)}$/kJ mol^{-1}	160.3	599.1	297.1	737.1
HOMO (eV)	−9.19	−9.53	−9.08	−9.31
LUMO (eV)	−0.70	−1.47	−0.91	−1.52
ΔE(HOMO–LUMO)$^{b)}$/eV	8.49	8.06	8.17	7.79
Net atomic charge on O(10)	−0.22	−0.22	−0.22	−0.22

a) Heat of formation. b) HOMO–LUMO energy gap.

Table 16.   Properties of the Anion Species $(\mathbf{IP} - \mathbf{H})^-$ of **1** and **2** Calculated with the AM1-COSMO Method ($\varepsilon = 46.5$)

	$(\mathbf{IP} - \mathbf{H})^-$ of **1**	$(\mathbf{IP} - \mathbf{H})^-$ of **2**
$\Delta H_f{}^{a)}$/kJ mol^{-1}	−272.6	−145.4
HOMO (eV)	−7.70	−7.65
LUMO (eV)	−0.29	−0.51
ΔE(HOMO–LUMO)$^{b)}$/eV	7.41	7.14
Net atomic charge on O(10)	−0.64	−0.59

a) Heat of formation. b) HOMO–LUMO energy gap.

the calculation results support the spectroscopic observations of the protonated species VII of **5** and **6**.

In the presence of TMG, a spectroscopic character of anion species $(\mathbf{IP} - \mathbf{H})^-$ of **1** and **2** was observed. As spectroscopic data, the lowest energy band of $(\mathbf{IP} - \mathbf{H})^-$ of **1** in DMSO showed a red-shift (8 nm) compared with that of the neutral species, while the lowest energy band of $(\mathbf{IP} - \mathbf{H})^-$ of **2** in DMSO showed a blue-shift (13 nm). To understand this property, AM1-COSMO calculations ($\varepsilon = 46.5$) of $(\mathbf{IP} - \mathbf{H})^-$ of **1** and **2** were carried out (Table 16), and gave the results that the HOMO–LUMO energy gaps of $(\mathbf{IP} - \mathbf{H})^-$ of **1** and **2** are 0.40 eV larger than those of the corresponding neutral molecules. This result cannot explain the spectroscopic observation. Thus, to predict the spectroscopic property of anion species $(\mathbf{IP} - \mathbf{H})^-$ correctly, the effect of a molecular environment must be considered further.

Based on spectroscopic observations, the π-electronic properties of the neutral molecules of **1**–**6**, the protonated species of **1**–**6**, and the anion species of **1** and **2** were categorized into a 'solvatochromic group' and a 'non-solvatochromic group'

(Scheme 4). The difference of the two groups is caused by the different π-electronic structures. A 'solvatochromic group' molecule has an imidazopyrazinone π-system containing the conjugated p orbital of O10, while a 'non-solvatochromic group' molecule has an imidazopyrazine π-system conjugating with the lone-pair electrons of O10. Since **1**–**4** and **5**–**6** are representative molecules of the 'solvatochromic group' and the 'non-solvatochromic group', respectively, the different MO characters between **1**–**4** and **5′**–**6′** obtained by AM1-COSMO calculations reflect the different π-electronic properties of the two groups, as follows. At first, the energy levels of the HOMOs of **1**–**4** (−7.91 to −7.96 eV) are higher than those of **5′** and **6′** (−9.08 to −9.19 eV). Secondly, the net atomic charges on O10 of **1**–**4** (−0.54 to −0.57) are smaller than those of **5′** and **6′** (−0.22). These different MO characters are applicable to distinguish the properties of the protonated species and the anion species. The protonated species VI of **1**–**4** and the anion species $(\mathbf{IP} - \mathbf{H})^-$ of **1** and **2** in the 'solvatochromic group' had calculated HOMO levels higher than −8.5 eV, and their net atomic charges on O10 were smaller than −0.5 (Table 14 and 16), while the protonated species V of **1**–**4** and the protonated species VII of **5′** and **6′** in the 'non-solvatochromic group' had HOMO levels lower than −9.0 eV and had a large net atomic charges on O10 (−0.22 to −0.27) (Table 14 and 15). The localized negative charges on O10 of the 'solvatochromic group' molecules would work for a hydrogen-bonding interaction with solvent molecules possessing a hydrogen-bond donor property. These evaluations indicate that for a classification of the π-electronic characters of the neutral molecules, the protonated species, and the anion species of imidazopyrazine derivatives it is useful to use the solvatochromic property as a criterion.

(f) Chemiluminescence Process: A chemiluminescence

Scheme 7.

Chart 5.

Chart 6.
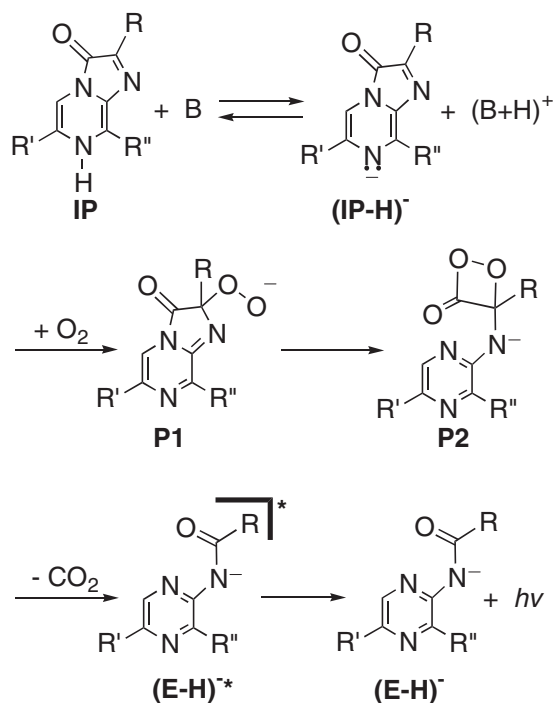
reaction of an imidazopyrazinone derivative proceeds via an anion species, as shown in Scheme 7.[5,7,8] After deprotonation of an imidazopyrazinone derivative (**IP**), an anion species (**IP − H**)⁻ reacts with molecular oxygen, since (**IP − H**)⁻ is more reactive with O_2 than the neutral molecule.[7–9,41] The reaction of (**IP − H**)⁻ and O_2 gives a peroxide intermediate **P1**,[42] followed by the generation of a dioxetanone intermediate **P2**. Dioxetanone **P2** decomposes to give a singlet excited state of amidopyrazine anion (**E − H**)⁻*, which emits light. In the reaction sequence, the formation of **P1** is supported by the results of a structure elucidation of aequorin[43] and a low-temperature oxygenation of imidazopyrazinone derivatives.[44,45] Thus, it is important to understand the reactivity of (**IP − H**)⁻ with O_2 to give peroxide **P1** for clarifying the mechanism of bio- and chemiluminescence reactions. In the reaction of (**IP − H**)⁻ with O_2, the HOMO of (**IP − H**)⁻ interacts with the LUMO of molecular oxygen. In the case of the anion species (**IP − H**)⁻ of **1**, the C2 position has the largest coefficient of HOMO to support the regioselective generation of **XV** (**P1** from **1**). As another oxygenated intermediates, a peroxide isomer **XVI** was postulated, which was a product oxygenated at C5,[46] while the coefficient of HOMO at C5 for (**IP − H**)⁻ of **1** is not so significant. Furthermore, the optimized heat of formation of **XV** (-293.4 kJ mol⁻¹) with the AM1-COSMO ($\varepsilon = 46.5$) is smaller than that of **XVI** (-276.5 kJ mol⁻¹). This result supports that the regioselective generation of **P1** is preferable in the bio- and chemiluminescence reactions and oxygenation of (**IP − H**)⁻ at C5 would be improbable.

(g) Chemiluminescence Experimental Condition: To investigate a chemiluminescence reactivity of an imidazopyrazinone derivative experimentally, a general procedure has been employed without any explanation. In this general procedure, a stock solution of an imidazopyrazinone derivative in an alcohol, such as methanol, is prepared, and a small portion of the
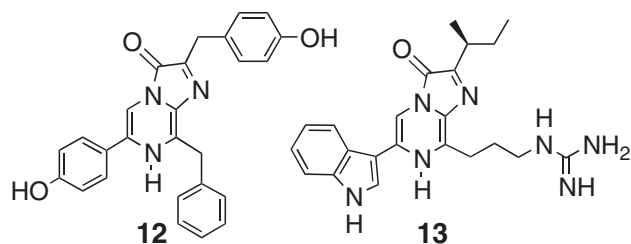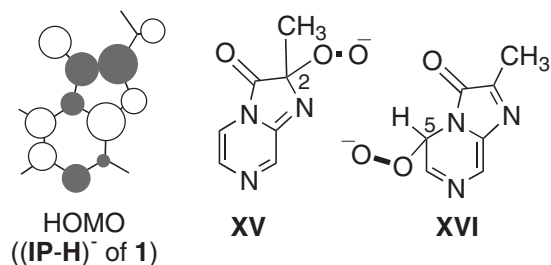
stock solution is mixed with a large volume of an aprotic solvent under O_2, resulting in an initiation of a chemiluminescence reaction.[47,48] As aprotic solvents, DMSO, DMF, and ethyleneglycol dimethyl ether, have been used.[5,8,49] Our results of this report can explain a reason to use this general procedure. In a stock solution in alcohol, an imidazopyrazinone derivative and its anion species (**IP − H**)⁻ are stabilized by solvent molecules with hydrogen-bonding interactions. Then, an imidazopyrazinone derivative becomes inert in alcohol, and it is easy to handle the stock solution. When the stock solution is mixed with an aprotic solvent, the stabilization effect by hydrogen-bonding interactions in alcohol is diluted, resulting in the generation of a reactive naked imidazopyrazinone molecule and its anion species (**IP − H**)⁻. Then, the naked anion species (**IP − H**)⁻ efficiently reacts with a molecular oxygen to undergo a chemiluminescence reaction.

(h) Molecular Recognition in Bioluminescence Reactions: As bioluminescent imidazopyrazinone derivatives, coelenterazine **12**[1,2] and *Cypridina* luciferin **13**[3–5] have been well studied. Coelenterazine **12** works as a luminescent substrate in aequorin bioluminescence, and **13** works as a luciferin in *Cypridina* bioluminescence. From the viewpoint of molecular recognition, the structures of the appendages to the imidazopyrazinone rings of **12**[47,50,51] and **13**[4,5] are important for regulating the bioluminescent activity. This means that the apoaequorin (apoprotein) and *Cypridina* luciferase precisely recognize the appendage structures of **12** and **13**, respectively, and promote their luminescent reaction with O_2 as the enzymatic processes. In addition to the molecular recognitions of the appendage structures of **12** and **13**, we would like to propose that the imidazopyrazinone rings, themselves, in **12** and **13** work as one of the important factors for molecular recognitions in bioluminescence reactions. To predict the properties of **12** and **13**, AM1-COSMO calculations ($\varepsilon = 46.5$) of simple model compounds **12′** and **13′** were carried out (Table 17). The optimized HOMO levels of **12′** and **13′** were higher than -8.0 eV, and the net atomic charges on O10 of **12′** and **13′** were optimized as -0.55 and -0.56, respectively. These calculated properties

Table 17.   Properties of Model Compounds **12′** and **13′** Calculated with the AM1-COSMO Method ($\varepsilon = 46.5$)

	12′	**13′**
ΔH_f[a)]/kJ mol^{-1}	15.1	326.3
HOMO (eV)	−7.98	−7.90
LUMO (eV)	−1.08	−1.08
ΔE(HOMO–LUMO)[b)]/eV	6.89	6.83
Charge on O(10)[c)]	−0.55	−0.56

a) Heat of formation.   b) HOMO–LUMO energy gap.   c) Net atomic charge on O(10).

are similar to those of simple imidazopyrazinone derivatives **1**–**4**, indicating that **12** and **13** keep the typical characteristics of the imidazopyrazinone π-system. Thus, **12** and **13** have a character of the zwitter-ionic resonance structures, like **II**, and an ability to make hydrogen-bonding interactions with a hydrogen-bond donor molecule at O10. For the molecular recognitions of **12** and **13** by apoaequorin and *Cypridina* luciferase, respectively, dipole–dipole interactions and hydrogen-bonding interactions may work as important bonding interactions.

Conclusions

The fundamental physical properties of **1**–**6** have been systematically investigated by X-ray crystallography, UV/vis absorption spectroscopy, NMR, and AM1-COSMO calculations, and have been evaluated by comparing to the reported data of Goto and others. As a structural characteristic observed by X-ray crystal structures **3** and **4**, their core imidazopyrazinone rings were virtually planar. These planar ring structures were reproduced by structure optimizations with AM1-COSMO calculations. The observed C3–O10 bond lengths and the ^{13}C chemical shifts of C3 for imidazopyrazinone derivatives indicate that the imidazopyrazinone structure has a weakened carbonyl character of the C3–O10 bonds. The reason for this structural characteristic is that the imidazopyrazinone π-system has a contribution of the zwitter-ionic resonance structure **II** possessing an aromatic 10 π-electron ring (Scheme 1). The ^{1}H NMR data of **1**–**4** support that the imidazopyrazinone rings have small portions of aromatic (diatropic) character. On the other hand, the NMR data of **5** and **6** indicate that their π-electron ring systems have a moderate aromatic (diatropic) character. UV/vis absorption measurements of **1**–**6** also indicated different π-electronic characters between **1**–**4** and **5**–**6**. Imidazopyrazinone derivatives **1**–**4** had the lowest energy bands in the visible wavelength region and solvatochromic character originated by a hydrogen-bonding interaction, while **5** and **6** had the lowest energy bands in the UV region and no solvatochromic character. The different π-electronic characters between **1**–**4** and **5**–**6** clarify that an N–H derivative, such as **1** and **2**, is preferable to be the NH form (**III**) over the OH form (**IV**) in the tautomeric equilibrium (Scheme 2). This conclusion is also supported by a quantitative evaluation of the protonation of **3**–**6** experimentally (Fig. 15 and 16). The observed

different spectroscopic characters between **1**–**4** and **5**–**6** were supported by AM1-COSMO calculations. For explaining the solvatochromism of **1**–**4**, we have described a hydrogen-bonded structure **XII** of an imidazopyrazinone derivative with a hydrogen-bond donor molecule (**D–H**) by using resonance structures **XIII** and **XIV** (Scheme 6). In structure **XII**, the oxygen atom O10 acts as a hydrogen-bond acceptor part, and interacts with solvent molecules with a hydrogen-bond donor property. The spectral shift dependent upon the Kamlet–Taft's α value of a solvent would be caused by a change in the contributions of **XIII** and **XIV** (Eq. 5).

Protonated species of **1**–**6** generated in the presence of methanesulfonic acid (MSA) were studied by UV/vis absorption and NMR measurements. The UV/vis absorption spectral changes gave the formation constants K for these protonations. Based on the assignment by the Goto group,[13d] the protonated species of **1**–**4** were assigned to structures **V** and **VI**, and the protonated species of **5** and **6** were assigned to structure **VII** (Scheme 3). As spectroscopic characteristics of the protonated species, **V** had the blue-shifted lowest energy bands compared with the corresponding neutral molecules, and **VI** had the red-shifted lowest energy bands. The protonated species **VII** of **5** and **6** showed the red-shifted lowest energy bands compared with the neutral molecules. These spectral changes are consistent with the calculated HOMO–LUMO energy gaps. In addition, protonated species **VI** showed solvatochromism originated by hydrogen-bonding interactions, while **V** and **VII** showed no solvatochromism. Anion species $(\mathbf{IP} - \mathbf{H})^-$ of **1** and **2** generated in the presence of 1,1,3,3-tetramethylguanidine (TMG) were characterized by UV/vis absorption and NMR measurements. As a spectroscopic characteristic, $(\mathbf{IP} - \mathbf{H})^-$ had the solvatochromic character originated by hydrogen-bonding interactions. The solvatochromic property originated by hydrogen-bonding interactions is useful as a criterion for categorizing the imidazopyrazine π-electron systems into two groups, solvatochromic and non-solvatochromic groups (Scheme 4). The participation of the p orbital of O10 into the imidazopyrazine π-system is important to regulate the π-electronic characters, inducing the solvatochromic behavior. The different π-electronic characters of these two groups were consistent with the different calculated MO characters.

The observed fundamental physical properties of imidazo-

pyrazinone derivatives and the MO calculation results explain the problems of the chemiluminescence reaction sequence, the experimental procedure for chemiluminescence reactions, supramolecule constructions in bioluminescence processes, and the reactivity of a bioluminescent substrate.

Experimental

General. Melting points were obtained with a Yamato MP-21 apparatus, and were used uncorrected. IR spectra were measured with a Horiba FT-720 spectrometer. Electron impact (EI) mass spectra were recorded with a JEOL JMS-600 mass spectrometer. High-resolution EI mass spectra were recorded with a JEOL HX-110 mass spectrometer. Elemental analysis was performed by the Instrumental Analyses Center for Chemistry, Graduate School of Science, Tohoku University. ^{1}H and ^{13}C NMR spectra were recorded on a JEOL GX-270 instrument (270 and 67.8 MHz, respectively). UV–visible absorption spectra were measured with a Varian Cary 50 spectrophotometer. Spectroscopic measurements were made in a quartz cuvette (1 cm path-length) at 25 ± 1 °C. Spectral-grade solvents were used to measure the UV/vis absorption spectra. Semi-empirical MO calculations were carried out with the AM1 Hamiltonian^{33} in the MOPAC package (MOPAC2000 ver. 1.0, Fujitsu Ltd, Tokyo, Japan, 1999). The geometric structures were fully optimized by AM1 calculations.

2-Methylimidazo[1,2-*a*]pyrazin-3(7*H*)-one (1). An HCl salt of **1** was prepared according to the reported procedure.^{12a,16} An HCl salt of **1** (200 mg, 1.08 mmol) in water (2 mL) was treated with K$_2$CO$_3$ (76 mg, 0.6 mmol) under Ar, and the product was purified by silica-gel column chromatography (chloroform/methanol = 5:1), yielding **1** (131 mg, 81%) as an orange powder; mp > 250 °C (dec.); IR (KBr) 3340, 3102, 3051, 2929, 1674, 1610, 1570, 1506, 1294, 1130 cm^{-1}; MS (EI, 70 eV) *m/z* (%) 149 (M$^+$, 100), 120 (25), 80 (58); Anal. Found: C, 55.36; H, 4.85; N, 27.60%. Calcd for C$_7$H$_7$N$_3$O·1/6H$_2$O: C, 55.26; H, 4.86; N, 27.62%. The NMR data are shown in the text.

2-Phenylimidazo[1,2-*a*]pyrazin-3(7*H*)-one (2). This compound was prepared according to the reported procedure.^{17} The product was purified by silica-gel column chromatography (chloroform/methanol = 10:1), to give **2** as red powder; mp > 250 °C (dec.); IR (KBr) 3342, 3226, 3143, 3103, 3018, 1664, 1612, 1564, 1236, 1128 cm^{-1}; MS (EI, 70 eV) *m/z* (%) 211 (M$^+$, 99), 182 (100), 103 (48), 80 (78); Anal. Found: C, 65.49; H, 4.52; N, 18.91%. Calcd for C$_{12}$H$_9$N$_3$O·1/2H$_2$O: C, 65.45; H, 4.58; N, 19.08%. The NMR data are shown in the text.

2,7-Dimethylimidazo[1,2-*a*]pyrazin-3(7*H*)-one (3). This compound was prepared according to the modified procedure reported in Ref. 13c. To a solution of **1**·HCl salt (251 mg, 1.35 mmol) and potassium carbonate (565 mg, 4.1 mmol) in water (2 mL), dimethyl sulfate (0.18 mL, 1.9 mmol) was added under Ar; the reaction mixture was stirred for 2 h at room temperature. The reaction was quenched by adding methanol (2 mL), and the solvent was removed in vacuo. The obtained yellow combined organic layers were dried over anhydrous Na$_2$SO$_4$, and concentrated in vacuo. The yellow residue was purified by silica-gel column chromatography (chloroform/methanol = 8:1), yielding **3** (149 mg, 68%) as yellow powder; mp 169.5–170.5 °C (lit.^{13c} 182 °C (dec.)); IR (KBr) 3448, 3257, 3062, 2947, 2920, 1684, 1591, 1576, 1130 cm^{-1}; MS (EI, 70 eV) *m/z* (%) 163 (M$^+$, 97), 94 (100); Anal. found: C, 52.72; H, 6.08; N, 22.94%. Calcd for C$_8$H$_9$N$_3$O·H$_2$O: C, 53.03; H, 6.12; N, 23.19%. The NMR data are shown in the text.

7-Methyl-2-phenylimidazo[1,2-*a*]pyrazin-3(7*H*)-one (4). To a solution of **2** (502 mg, 2.38 mmol) and methyl iodide (0.44 mL, 7.1 mmol) in DMF (3 mL), potassium carbonate (0.98 g, 7.1 mmol) was added under Ar. The reaction mixture was stirred for 20 min at room temperature, and the reaction mixture was diluted with AcOEt. The organic layer was washed with water and brine, and was dried over anhydrous Na$_2$SO$_4$. After removing the solvent in vacuo, the dark-red residue was purified by silica-gel column chromatography (chloroform/methanol = 10:1), yielding **4** (371 mg, 69%) as red needles; mp > 250 °C (dec.); IR (KBr) 3087, 3053, 3028, 3005, 2933, 1670, 1599, 1240, 1124 cm^{-1}; MS (EI, 70 eV) *m/z* (%) 225 (M$^+$, 81), 94 (100); Anal. Found: C, 69.55; H, 5.00; N, 18.72%. Calcd for C$_{13}$H$_{11}$N$_3$O: C, 69.32; H, 4.92; N, 18.66%. The NMR data are shown in the text.

3-Ethoxy-2-methylimidazo[1,2-*a*]pyrazine (5). To a solution of **1**·HCl salt (501 mg, 2.70 mmol) and ethyl iodide (1.0 mL, 1.9 mmol) in a mixture of DMF (3 mL) and water (0.5 mL), potassium carbonate (1.34 g, 9.7 mmol) was added under Ar, and the reaction mixture was stirred for 1 h at room temperature. The solvent was removed in vacuo, and the residue suspended in a mixture of EtOH–AcOEt was filtered through filter paper. The filtrate was concentrated in vacuo and purified by silica-gel column chromatography (chloroform/methanol = 30:1 to 10:1), yielding **5** (250 mg, 52%) as pale-yellow needles accompanied by 7-ethyl-2-methylimidazo[1,2-*a*]pyrazin-3(7*H*)-one (135 mg, 28%) as an orange powder. Compound **5**; mp 70.0–71.0 °C; IR (KBr) 3016, 2981, 2911, 1618, 1558, 1354, 1230 cm^{-1}; MS (EI, 70 eV) *m/z* (%) 177 (M$^+$, 85), 148 (48), 120 (100), 79 (60); Anal. Found: C, 60.90; H, 6.23; N, 23.59%. Calcd for C$_9$H$_{11}$N$_3$O: C, 61.00; H, 6.26; N, 23.71%. The NMR data are shown in the text.

7-Ethyl-2-methylimidazo[1,2-*a*]pyrazin-3(7*H*)-one: mp 92.0–94.0°C; IR (KBr) 3437, 3242, 3062, 2993, 2943, 2920, 1684, 1593, and 1126 cm^{-1}; ^{1}H NMR (DMSO-d_6) δ 1.29 (3H, t, J = 7.3 Hz), 2.27 (3H, s), 3.79 (2H, q, J = 7.3 Hz), 6.79 (1H, dd, J = 1.3, 5.9 Hz), 7.21 (1H, d, J = 5.9 Hz), and 7.79 (1H, brs); MS (EI, 70 eV) *m/z* (%) 177 (M$^+$, 81), 108 (100).

3-Ethoxy-2-phenylimidazo[1,2-*a*]pyrazine (6). This compound was prepared according to a procedure analogous to that of **5** in 46% yield, accompanied by 7-ethyl-2-phenylimidazo[1,2-*a*]pyrazin-3(7*H*)-one (29%). Compound **6**; pale-brown needles; mp 94.0–95.0 °C; IR (KBr) 3051, 3024, 2983, 2939, 2897, 1604, 1576, 1549, 1489, 1360, 1200, 1020 cm^{-1}; MS (EI, 70 eV) *m/z* (%) 239 (M$^+$, 52), 210 (28), 182 (100), 79 (33); Anal. Found: C, 70.57; H, 5.56; N, 17.64%. Calcd for C$_{14}$H$_{13}$N$_3$O: C, 70.28; H, 5.48; N, 17.56%. The NMR data are shown in the text.

7-Ethyl-2-phenylimidazo[1,2-*a*]pyrazin-3(7*H*)-one: red powder; mp 199.0–202.0 °C; IR (KBr) 3055, 3026, 2983, 2933, 1670, 1620, 1589, 1242, and 1124 cm^{-1}; ^{1}H NMR (DMSO-d_6) δ 1.36 (3H, t, J = 7.3 Hz), 3.92 (2H, q, J = 7.3 Hz), 6.95 (1H, dd, J = 1.3, 5.9 Hz), 7.34 (1H, m), 7.45 (2H, m), 7.51 (1H, d, J = 5.9 Hz), 8.16 (1H, d, J = 1.0 Hz), and 8.47 (2H, m); MS (EI, 70 eV) *m/z* (%) 239 (M$^+$, 70), 108 (100).

X-ray Crystallography. Crystals of **3** were obtained by slow evaporation from a solution in a mixture of acetone, water, and diethyleneglycol dimethyl ether as yellow prisms; Anal. Found: C, 42.75; H, 7.02; N, 18.69%. Calcd for C$_8$H$_9$N$_3$O·7/2H$_2$O: C, 42.47; H, 7.13; N, 18.57%. Crystals of **4** were grown from the solution in a mixture of 1-propanol, water, and hexane as red prisms. Crystal data and details of the refinements are summarized in Table 1. The intensity data were measured using a Rigaku diffractometer (AFC-7R) with a graphite monochromator. Because crystals of **3** were fairly unstable in the air at room temperature, they

were sealed in an epoxy resin and an intensity measurement was carried out at 110 K with an N_2-extraction gas-flow device. Absorption corrections were applied by the Ψ-scan method[52] for **3**. The structures were solved by a direct method using the program MITHRIL90.[53] In crystal **3**, four water molecules were found in the successive Fourier map. One water molecule lies on the crystallographic 2-fold axis, so that the hydrogen atoms of this water molecule are statically disordered. Other water molecules also show a static disorder as one hydrogen atom of each water molecule distributes on two positions. The positions of all the H atoms were obtained from D-maps. The structures were refined by full-matrix least-squares with anisotropic temperature factors for non-H atoms and isotropic ones for H atoms. The final *R* values are 0.0294 and 0.0405 for 2369 and 4019 observed reflections with $I > 2\sigma(I)$ for **3** and **4**, respectively.[54] Atomic-scattering factors were taken from International Tables for X-Ray Crystallography.[55] Computations were performed using the programs teXsan,[56] SHELXL-97,[57] WINGX,[58] and ORTEP3 for Windows.[59]

References

1 a) O. Shimomura, F. H. Johnson, and Y. Saiga, *J. Cell. Comp. Physiol.*, **59**, 223 (1962). b) F. H. Johnson and O. Shimomura, *Methods Enzymol.*, **57**, 71 (1978).

2 Y. Ohmiya and T. Hirano, *Chem. Biol.*, **3**, 337 (1996).

3 Y. Kishi, T. Goto, Y. Hirata, O. Shimomura, and F. H. Johnson, *Tetrahedron Lett.*, **7**, 3427 (1966).

4 H. Nakamura, M. Aizawa, D. Takeuchi, A. Murai, and O. Shimomura, *Tetrahedron Lett.*, **41**, 2185 (2000).

5 a) T. Goto, *Pure Appl. Chem.*, **17**, 421 (1968). b) T. Goto, M. Isobe, D. A. Coviello, Y. Kishi, and S. Inoue, *Tetrahedron*, **29**, 2035 (1973).

6 a) M. Isobe, T. Fujii, S. Swan, M. Kuse, K. Tsuboi, A. Miyazaki, M. C. Feng, and J. Li, *Pure Appl. Chem.*, **70**, 2085 (1998). b) M. Kuse and M. Isobe, *Tetrahedron*, **56**, 2629 (2000).

7 F. McCapra and Y. C. Chang, *J. Chem. Soc., Chem. Commun.*, **1967**, 1011.

8 T. Goto and Y. Kishi, *Angew. Chem., Int. Ed. Engl.*, **7**, 407 (1968).

9 T. Hirano, Y. Gomi, T. Takahashi, K. Kitahara, F. Q. Chen, I. Mizoguchi, S. Kyushin, and M. Ohashi, *Tetrahedron Lett.*, **39**, 5771 (1992).

10 a) R. Saito, T. Hirano, and M. Ohashi, *J. Chem. Soc., Perkin Trans. 2*, **1997**, 1711. b) R. Saito, T. Hirano, H. Niwa, and M. Ohashi, *Chem. Lett.*, **1998**, 95.

11 T. Hirano, S. Nishibuchi, M. Yoneda, K. Tsujimoto, and M. Ohashi, *Tetrahedron*, **49**, 9267 (1993).

12 a) I. Devillers, B. de Wergifosse, M.-P. Bruneau, B. Tinant, J.-P. Declercq, R. Touillaux, J.-F. Ress, and J. Marchand-Brynaert, *J. Chem. Soc., Perkin Trans. 2*, **1999**, 1481. b) M. L. N. Dubuisson, B. de Wergifosse, A. Trouet, F. Baguet, J. Marchand-Brynaert, and J.-F. Ress, *Biochem. Pharmacol.*, **60**, 471 (2000). c) M. L. N. Dubuisson, B. de Wergifosse, P. Kremers, J. Marchand-Brynaert, A. Trouet, and J.-F. Ress, *Free Radical Res.*, **34**, 285 (2001). d) I. Devillers, G. Dive, C. de Tollenaere, B. Falmagne, B. de

Wergifosse, J.-F. Ress, and J. Marchand-Brynaert, *Bioorg. Med. Chem. Lett.*, **11**, 2305 (2001).

13 a) T. Goto, S. Inoue, and S. Sugiura, *Tetrahedron Lett.*, **9**, 3873 (1968). b) S. Sugiura, S. Inoue, and T. Goto, *Yakugaku Zasshi*, **90**, 423 (1970). c) S. Sugiura, S. Inoue, and T. Goto, *Yakugaku Zasshi*, **90**, 431 (1970). d) T. Goto, M. Isobe, Y. Kishi, S. Inoue, and S. Sugiura, *Tetrahedron*, **31**, 939 (1975).

14 K. Hori, J. M. Anderson, W. W. Ward, and M. J. Cormier, *Biochemistry*, **14**, 2371 (1975).

15 B. Alcaide, J. Plumet, M. A. Sierra, and C. Vincent, *J. Org. Chem.*, **54**, 5763 (1989).

16 S. Inoue, S. Sugiura, H. Kakoi, and T. Goto, *Tetrahedron Lett.*, **10**, 1609 (1969).

17 G. B. Barlin, D. J. Brown, Z. Kadunc, A. Petric, B. Stanovnik, and M. Tisler, *Aust. J. Chem.*, **36**, 1215 (1983).

18 R. Nelson and L. Pierce, *J. Mol. Spectrosc.*, **18**, 344 (1965).

19 M. J. Barrow and O. S. Mills, *J. Chem. Soc., Chem. Commun.*, **1973**, 66.

20 V. I. Minkin, M. N. Glukhovtsev, and B. Ya. Simkin, "Aromaticity and Antiaromaticity—Electronic and Structural Aspects," John Wiley & Sons, New York (1994).

21 P. Vlček, Z. Havlas, and Z. Pavlíček, *Collect. Czech. Chem. Commun.*, **64**, 633 (1999).

22 G. De With, S. Harkema, and D. Feil, *Acta Crystallogr., Sect. B*, **32**, 3178 (1976).

23 H.-D. Hausen, O. Mundt, and W. Kaim, *J. Organomet. Chem.*, **296**, 321 (1985).

24 R. Ludwig, *Angew. Chem., Int. Ed.*, **40**, 1808 (2001).

25 C. Reichardt, "Solvents and Solvent Effects in Organic Chemistry," 2nd ed, VCH, Weinheim (1990).

26 a) R. W. Taft and M. J. Kamlet, *J. Am. Chem. Soc.*, **98**, 2886 (1976). b) M. J. Kamlet and R. W. Taft, *J. Am. Chem. Soc.*, **98**, 377 (1976). c) M. J. Kamlet, J.-L. M. Abboud, and R. W. Taft, *J. Am. Chem. Soc.*, **99**, 6027 (1977). d) M. J. Kamlet, J.-L. M. Abboud, M. H. Abraham, and R. W. Taft, *J. Org. Chem.*, **48**, 2877 (1983).

27 H. J. Schneider and A. Yatsimirsky, "Principles and Methods in Supramolecular Chemistry," John Wiley & Sons, Chichester (2000).

28 F. Uchimaru, S. Okada, A. Kosasayama, and T. Konno, *Chem. Pharm. Bull.*, **20**, 2204 (1972).

29 a) W. Kaim, *Angew. Chem., Int. Ed. Engl.*, **20**, 599 (1981). b) W. Kaim, *J. Am. Chem. Soc.*, **105**, 707 (1983).

30 A. Ehlend, H.-D. Hausen, W. Kaim, A. Lichtblau, and W. Schwarz, *J. Organomet. Chem.*, **501**, 283 (1995).

31 H.-O. Kalinowski, S. Berger, and S. Braun, "Carbon-13 NMR Spectroscopy," John Wiley & Sons, Chichester (1984).

32 A. Lichtblau, A. Ehlend, H.-D. Hausen, and W. Kaim, *Chem. Ber.*, **128**, 745 (1995).

33 M. J. S. Dewar, E. G. Zoebisch, E. F. Healy, and J. J. P. Stewart, *J. Am. Chem. Soc.*, **107**, 3902 (1985).

34 A. Klant and G. Shuurmann, *J. Chem. Soc., Perkin Trans. 2*, **1993**, 799.

35 A. D. Giacomo and C. P. Smyth, *J. Am. Chem. Soc.*, **74**, 4411 (1952).

36 Y. Kurita, S. Seto, T. Nozoe, and M. Kubo, *Bull. Chem. Soc. Jpn.*, **26**, 272 (1953).

37 J. M. Clayton, G. E. Bass, W. P. Purcell, and C. C. Thompson, *J. Pharm. Sci.*, **63**, 230 (1974).

38 A. Schweig, *Z. Naturforsch., A*, **22A**, 724 (1967).

39 C. A. Coulson, *Research*, **10**, 149 (1957).

40 H. Umeyama and K. Morokuma, *J. Am. Chem. Soc.*, **99**, 1316 (1977).

41   K. Fujimori, H. Nakajima, K. Akutsu, M. Mitani, H. Sawada, and M. Nakayama, *J. Chem. Soc., Perkin Trans. 2*, **1993**, 2405.

42   O. Shimomura and F. H. Johnson, *Biochem. Biophys. Res. Commun.*, **44**, 340 (1971).

43   a) B. Musicki, Y. Kishi, and O. Shimomura, *J. Chem. Soc., Chem. Commun.*, **1986**, 1566. b) J. H. Head, S. Inouye, K. Teranishi, and O. Shimomura, *Nature*, **405**, 372 (2000).

44   K. Teranishi, K. Ueda, H. Nakao, M. Hisamitsu, and T. Yamada, *Tetrahedron Lett.*, **35**, 8181 (1994).

45   K. Usami and M. Isobe, *Tetrahedron*, **52**, 12061 (1996).

46   a) K. Teranishi, M. Isobe, T. Yamada, and T. Goto, *Tetrahedron Lett.*, **33**, 1303 (1992). b) K. Teranishi, M. Hisamitsu, and T. Yamada, *Tetrahedron Lett.*, **37**, 8425 (1996).

47   a) F. Q. Chen, Y. Gomi, T. Hirano, M. Ohashi, Y. Ohmiya, and F. I. Tsuji, *J. Chem. Soc., Perkin Trans. 1*, **1992**, 1607. b) T. Hirano, R. Negishi, M. Yamaguchi, F. Q. Chen, Y. Ohmiya, F. I. Tsuji, and M. Ohashi, *Tetrahedron*, **53**, 12903 (1997).

48   Y. Toya, T. Kayano, K. Sato, and T. Goto, *Bull. Chem. Soc. Jpn.*, **65**, 2475 (1992).

49   K. Teranishi and T. Goto, *Bull. Chem. Soc. Jpn.*, **63**, 3132 (1990).

50   a) O. Shimomura, B. Musicki, and Y. Kishi, *Biochem. J.*, **251**, 405 (1988). b) O. Shimomura, B. Musicki, and Y. Kishi, *Biochem. J.*, **261**, 913 (1989). c) O. Shimomura, S. Inouye, B. Musicki, and Y. Kishi, *Biochem. J.*, **270**, 309 (1990). d) O. Shimomura, *Cell Calcium*, **12**, 635 (1991). e) O. Shimomura, B. Musicki, Y. Kishi, and S. Inouye, *Cell Calcium*, **14**, 373 (1993). f) O. Shimomura, *Biochem. J.*, **306**, 537 (1995).

51   a) Y. Ohmiya, M. Ohashi, and F. I. Tsuji, *FEBS Lett.*, **301**, 197 (1992). b) Y. Ohmiya, K. Teranishi, M. Akutagawa, M. Ohashi, and F. I. Tsuji, *Chem. Lett.*, **1993**, 2149. c) T. Hirano, Y. Ohmiya, S. Maki, H. Niwa, and M. Ohashi, *Tetrahedron Lett.*, **39**, 5541 (1998).

52   A. C. T. North, D. C. Phillips, and F. S. Mathews, *Acta Crystallogr., Sect. A*, **A24**, 351 (1968).

53   C. J. Gilmore, *J. Appl. Crystallogr.*, **17**, 42 (1980).

54   Crystallographic data have been deposited at the CCDC, 12 Union Road, Cambridge CB2 1EZ, UK and copies can be obtained on request, free of charge, by quoting the publication citation and the deposition numbers 218058 and 218059.

55   "International Tables for Crystallography," ed by A. J. C. Wilson, Kluwer Academic Publishers, Dordrecht, The Netherlands (1995), Vol. C.

56   Molecular Structure Corporation, "teXsan. Single Crystal Structure Analysis Software," The Woodlands, TX (1993).

57   G. M. Sheldrick, "SHELXL-97. Program for crystal structure determination," In University of Göttingen, Germany (1997).

58   L. J. J. Farrugia, *Appl. Crystallogr.*, **32**, 837 (1999).

59   L. J. J. Farrugia, *Appl. Crystallogr.*, **30**, 565 (1997).